
Equivariant Hypergraph Diffusion Neural Operators

Peihao Wang^{1*}, Shenghao Yang², Yunyu Liu³, Zhangyang Wang¹, Pan Li^{3*}

¹University of Texas at Austin, ²University of Waterloo, ³Purdue University
 {peihao.wang, atlas.wang}@utexas.edu, shenghao.yang@uwaterloo.ca,
 {liu3154, panli}@purdue.edu

Abstract

Hypergraph neural networks (HNNs) using neural networks to encode hypergraphs provide a promising way to model higher-order relations in data and further solve relevant prediction tasks built upon such higher-order relations. However, higher-order relations in practice contain complex patterns and are often highly irregular. So, it is often challenging to designing an HNN that suffices to express those relations while keeping computational efficiency. Inspired by hypergraph diffusion algorithms, this work proposes a new HNN architecture named ED-HNN, which provably represents any continuous equivariant hypergraph diffusion operators that can model a wide range of higher-order relations. ED-HNN can be implemented efficiently by combining star expansions of hypergraphs with standard message passing neural networks. ED-HNN further shows great superiority in processing heterophilic hypergraphs and constructing deep models. We evaluate ED-HNN for node classification on nine real-world hypergraph datasets. ED-HNN¹ uniformly outperforms the best baselines over these nine datasets and achieves more than 2%[↑] in prediction accuracy over four datasets therein.

1 Introduction

Machine learning on graphs has recently attracted great attention in the community due to the ubiquitous graph-structured data and the associated inference and prediction problems [1–6]. Current works primarily focus on graphs which can model only pairwise relations in data. However, emerging research has shown that higher-order relations that involve more than two entities often reveal more significant information in many applications [7–11]. For example, higher-order network motifs build the fundamental blocks of many real-world networks [12–16]. Session-based (multi-step) behaviors often indicate the preferences of web users in more precise ways [17–20]. To capture these higher-order relations, hypergraphs provide a dedicated mathematical abstraction [21]. However, learning algorithms on hypergraphs are still far underdeveloped as opposed to those on graphs.

Recently, inspired by the success of graph neural networks (GNNs), researchers have started investigating hypergraph neural network models (HNNs) [22–30]. Compared with GNNs, designing HNNs is more challenging. First, as aforementioned, higher-order relations modeled by hyperedges could contain very complex information. Second, hyperedges in real-world hypergraphs are often of large and irregular sizes. Therefore, how to effectively represent higher-order relations while efficiently processing those irregular hyperedges is the key question to answer when one is to design HNNs. Unfortunately, just as other types of neural networks (NNs), HNNs look like a black box. Given an HNN, one can hardly tell the type of relations that it can represent and thus often fails to make a suitable tradeoff between the expressiveness and the computational efficiency of the model.

In this work, inspired by the recently developed hypergraph diffusion algorithms [31–38], we design a novel HNN architecture that holds provable expressiveness to represent a large class of hypergraph

*Correspondence to: Peihao Wang and Pan Li.

¹Our code is available at: <https://github.com/Graph-COM/ED-HNN>.

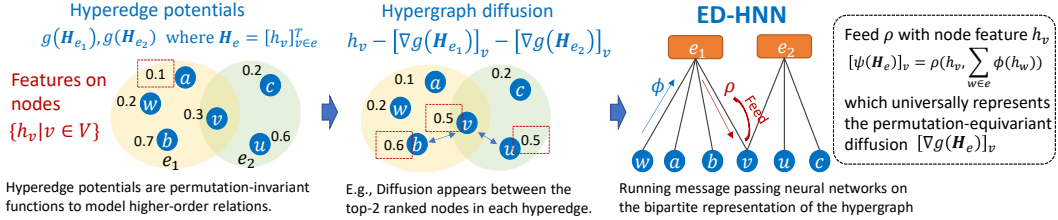


Figure 1: Hypergraph diffusion often uses permutation-invariant hyperedge potentials to model higher-order relations. The gradients or their variants of those potentials determine the diffusion process and are termed diffusion operators. Our ED-HNN can universally represent such operators by feeding node representations into the message from hyperedges to nodes.

diffusion while keeping computational efficiency. Hypergraph diffusion is significant due to its transparency and has been widely applied to clustering [16, 31, 39], semi-supervised learning [32, 37, 38, 40], ranking aggregation [16, 41], network analysis [33–36] and signal processing [8, 42–44]. However, traditional hypergraph diffusion needs to first handcraft potential functions to model higher-order relations and then use their gradients or some variants of their gradients as the diffusion operators to characterize the exchange of diffused quantities on the nodes within one hyperedge. The design of those potential functions often requires significant insights into the applications, which may not be available in practice.

We observe that the most commonly-used hyperedge potential functions are permutation invariant, which covers the applications where none of the nodes in a higher-order relation are treated as inherently special. We further show that their induced diffusion operators must be permutation equivariant. Inspired by this observation, we propose a NN-parameterized permutation-equivariant architecture that is expressive to provably represent any continuous hyperedge diffusion operators, whose NN parameters can be learned in a data-driven way. We also introduce an efficient implementation of the architecture via current GNN platforms [45, 46], which just needs to combine a bipartite representation (or star expansion [47, 48], equivalently) of hypergraphs and the standard message passing neural network (MPNN) [49]. By repeating this architecture by layers with shared parameters, we finally obtain our model Equivariant Diffusion-based HNN (ED-HNN). Fig. 1 shows an illustration of hypergraph diffusion and the key architecture in ED-HNN.

To the best of our knowledge, we are the first one to establish the connection between the general class of hypergraph diffusion algorithms and the design of HNNs. Previous HNNs were either less expressive to represent equivariant diffusion operators [22–27] or needed to learn the representations by adding significantly many auxiliary nodes [28–30]. We provide detailed discussion of them in Sec. 3.4. We also show that due to the equivariant architecture, ED-HNN is by design good at predicting node labels over heterophilic hypergraphs where hyperedges mix nodes from different classes. Moreover, ED-HNN can go very deep without much performance decay.

As a by-product, our proof of expressiveness does not use equivariant polynomials as a bridge, which were used previously in set-function approximation [50–52]. Our statement allows precise representations of continuous equivariant set functions by composing a continuous function and the sum of another continuous function on each set entry, while previous works have only achieved an approximation result. This result may be of independent interest for the community.

We evaluate ED-HNN by performing node classification over 9 real-world hypergraph datasets. ED-HNN uniformly outperforms all baseline methods in averaged performance and achieves significant improvement (more than 2% \uparrow) over 4 datasets therein. ED-HNN also shows super robustness when going deep. We further carefully design synthetic experiments to demonstrate the expressiveness of ED-HNN and the superiority of ED-HNN in processing heterophilic hypergraphs.

2 Preliminaries: Hypergraphs and Hypergraph Diffusion

In this section, we formulate the hypergraph diffusion problem, along the way, introduce the notations.

Definition 1 (Hypergraph). *Let $\mathcal{G} = (\mathcal{V}, \mathcal{E}, \mathbf{X})$ be an attributed hypergraph where \mathcal{V} is the node set of size N and \mathcal{E} is the hyperedge set of size M . Each hyperedge $e = \{v_1^{(e)}, \dots, v_{|e|}^{(e)}\}$ is a subset of \mathcal{V} . Unlike graphs, a hyperedge may contain more than two nodes. $\mathbf{X} = [\dots, \mathbf{x}_v, \dots]^T \in \mathbb{R}^N$ denotes the*

node attributes and \mathbf{x}_v denotes the attribute of node v . Define $d_v = |\{e \in \mathcal{E} : v \in e\}|$ as the degree of node v . Let \mathbf{D} , \mathbf{D}_e denote the diagonal degree matrix for $v \in \mathcal{V}$ and the sub-matrix for $v \in e$.

Here, we use 1-dim attributes for convenient discussion while our experiments often have multi-dim attributes. Learning algorithms will combine attributes and hypergraph structures into (latent) features defined as follows. These features can be further used to make prediction for downstream tasks.

Definition 2 (Latent features). Let $\mathbf{h}_v \in \mathbb{R}$ denote the (latent) features of node $v \in \mathcal{V}$. The feature vector $\mathbf{H} = [\dots, \mathbf{h}_v, \dots]_{v \in \mathcal{V}}^\top \in \mathbb{R}^N$ includes node features as entries. Further, collect the features into a edge feature vector $\mathbf{H}_e = [\mathbf{h}_{e,1} \ \cdots \ \mathbf{h}_{e,|e|}]^\top \in \mathbb{R}^{|e|}$, where $\mathbf{h}_{e,i}$ corresponds to the feature $\mathbf{h}_{v_i^{(e)}}$ for some node $v_i^{(e)} \in e$. Note that for any $v \in e$, there is one corresponding index $i \in \{1, \dots, |e|\}$. Later, we may use subscripts (e, i) and (e, v) interchangeably if they cause no confusion.

A widely-used heuristic to generate features \mathbf{H} is via hypergraph diffusion algorithms.

Definition 3 (Hypergraph Diffusion). Define node potential functions $f(\cdot; \mathbf{x}_v) : \mathbb{R} \rightarrow \mathbb{R}$ for $v \in \mathcal{V}$ and hyperedge potential functions $g_e(\cdot) : \mathbb{R}^{|e|} \rightarrow \mathbb{R}$ for each $e \in \mathcal{E}$. The hypergraph diffusion combines the node attributes and the hypergraph structure and asks to solve

$$\min_{\mathbf{H}} \sum_{v \in \mathcal{V}} f(\mathbf{h}_v; \mathbf{x}_v) + \sum_{e \in \mathcal{E}} g_e(\mathbf{H}_e). \quad (1)$$

In practice, g_e is often shared across hyperedges of the same size. Later, we ignore the subscript e .

The two potential functions are often designed via heuristics in traditional hypergraph diffusion literatures. Node potentials often correspond to some negative-log kernels of the latent features and the initial attributes. For example, $f(\mathbf{h}_v; \mathbf{x}_v)$ could be $(\mathbf{h}_v - \mathbf{x}_v)_2^2$ when to compute hypergraph PageRank diffusion [33, 36] or $-\mathbf{x}_v \mathbf{h}_v$ which essentially computes hypergraph min-cut [53–55]. Hyperedge potentials are more significant and complex, as they need to model those higher-order relations between more than two objects. Here list a few examples.

Example 1 (Hyperedge potentials). Some practical $g(\mathbf{H}_e)$ may be chosen as follows.

- *Clique Expansion (CE, hyperedges reduced to cliques) plus pairwise potentials* [31]: $\sum_{u,v \in e} (\mathbf{h}_v - \mathbf{h}_u)_2^2$ or with properly degree normalization $\sum_{u,v \in e} (\frac{\mathbf{h}_v}{\sqrt{d_v}} - \frac{\mathbf{h}_u}{\sqrt{d_u}})_2^2 (\triangleq g(\mathbf{D}_e^{-1/2} \mathbf{H}_e))$.
- *Divergence to the mean* [38, 56]: $\sum_{v \in e} (\mathbf{h}_v - \|\mathbf{H}_e\|_p^{-1} \mathbf{H}_e)_p^2$, where $\|\cdot\|_p$ computes the ℓ_p -norm.
- *Total Variation (TV)* [32, 36, 37]: $\max_{u,v \in e} |\mathbf{h}_v - \mathbf{h}_u|^p$, $p \in \{1, 2\}$.
- *Lovász Extension* [57] for cardinality-based set functions (LEC) [33, 34, 39, 54]: $\langle \mathbf{y}, \varsigma(\mathbf{H}_e) \rangle^p$, $p \in \{1, 2\}$ where $\mathbf{y} = [\dots, \mathbf{y}_j, \dots]^\top \in \mathbb{R}^{|e|}$ is a constant vector and $\varsigma(\mathbf{H}_e)$ sorts the values of \mathbf{H}_e in a decreasing order.

One may reproduce TV by using LEC and setting $\mathbf{y}_1 = -\mathbf{y}_{|e|} = 1$. To reveal more properties of these hyperedge potentials $g(\cdot)$, we list the following formal definitions.

Definition 4 (Permutation Invariance & Equivariance). Function $\psi : \mathbb{R}^K \rightarrow \mathbb{R}$ is permutation-invariant if for any K -dim permutation matrix $\mathbf{P} \in \Pi[K]$, $\psi(\mathbf{P}\mathbf{Z}) = \psi(\mathbf{Z})$ for all $\mathbf{Z} \in \mathbb{R}^K$. Function $\psi : \mathbb{R}^K \rightarrow \mathbb{R}^K$ is permutation-equivariant if for any K -dim permutation matrix $\mathbf{P} \in \Pi[K]$, $\psi(\mathbf{P}\mathbf{Z}) = \mathbf{P}\psi(\mathbf{Z})$ for all $\mathbf{Z} \in \mathbb{R}^K$.

We may easily verify permutation invariance of the hyperedge potentials in Example 1. The physical meaning behind this observation is that the prediction goal of an application is often independent of node identities in a hyperedge so practical g 's often keep invariant w.r.t. the node ordering [58].

3 Neural Equivariant Diffusion Operators and ED-HNN

Previous design of hyperedge potential functions is tricky. Early works adopted clique or star expansion by reducing hyperedges into (weighted) edges [16, 31, 47] and further used traditional graph methods. Later, researchers proved that those hyperedge reduction techniques cannot well represent higher-order relations [16, 59]. Therefore, Lovász extensions of set-based cut-cost functions

on hyperedges have been proposed recently used as the potential functions [32–36, 39, 60]. However, designing those set-based cut cost is practically hard and needs a lot of trials and errors. Other types of handcrafted hyperedge potentials to model information propagation can be found in [61, 62].

Our idea uses data-driven approaches to model such potentials, which naturally brings us to HNNs. On one hand, we expect to leverage the extreme expressive power of NNs to learn the desired hypergraph diffusion automatically from the data. On the other hand, we are interested in having novel hypergraph NN (HNN) architectures inspired by traditional hypergraph diffusion solvers.

To achieve the goals, next, we show by the gradient descent algorithm (GD) or alternating direction method of multipliers (ADMM) [63], solving objective Eq. 1 amounts to iteratively applying some hyperedge diffusion operators. Parameterizing such operators using NNs by each step can unfold hypergraph diffusion into an HNN. We make the key observation that the diffusion operators are inherently *permutation-equivariant*. To universally represent them, we propose a standard form to design equivariant NN-based operators and use it to build ED-HNN via an efficient implementation.

3.1 Emerging Equivariance in Hypergraph Diffusion

We start with discussing the traditional solvers for Eq. 1. If f and g are both differentiable, one straightforward optimization approach is to adopt gradient descent. The node-wise update of each iteration can be formulated as below:

$$\mathbf{h}_v^{(t+1)} \leftarrow \mathbf{h}_v^{(t)} - \eta(\nabla f(\mathbf{h}_v^{(t)}; \mathbf{x}_v) + \sum_{e:v \in e} [\nabla g(\mathbf{H}_e^{(t)})]_v), \quad \text{for } v \in \mathcal{V}, \quad (2)$$

where $[\nabla g(\mathbf{H}_e)]_v$ denotes the gradient w.r.t. \mathbf{h}_v for $v \in e$. We use the superscript t to denote the number of the current iteration, $\mathbf{h}_v^{(0)} = \mathbf{x}_v$ is the initial features, and η is known as the step size.

For general f and g , we may adopt ADMM [63]: For each $e \in \mathcal{E}$, we introduce an auxiliary variable $\mathbf{Q}_e = [\mathbf{q}_{e,1} \ \cdots \ \mathbf{q}_{e,|e|}]^\top \in \mathbb{R}^{|e|}$. We initialize $\mathbf{h}_v^{(0)} = \mathbf{x}_v$ and $\mathbf{Q}_e^{(0)} = \mathbf{H}_e^{(0)}$. And then, iterate

$$\mathbf{Q}_e^{(t+1)} \leftarrow \mathbf{prox}_{\eta g}(2\mathbf{H}_e^{(t)} - \mathbf{Q}_e^{(t)}) - \mathbf{H}_e^{(t)} + \mathbf{Q}_e^{(t)}, \quad \text{for } e \in \mathcal{E}, \quad (3)$$

$$\mathbf{h}_v^{(t+1)} \leftarrow \mathbf{prox}_{\eta f(\cdot; \mathbf{x}_v)/d_v}(\sum_{e:v \in e} \mathbf{q}_{e,v}^{(t+1)}/d_v), \quad \text{for } v \in \mathcal{V}, \quad (4)$$

where $\mathbf{prox}_\psi(\mathbf{h}) \triangleq \arg \min_{\mathbf{z}} \psi(\mathbf{z}) + \frac{1}{2} \|\mathbf{z} - \mathbf{h}\|_2^2$ is the proximal operator. The detailed derivation can be found in Appendix A. Note that previous hypergraph diffusion algorithms based on primal-dual hybrid gradient descent [32] or alternative projection [33, 55] for some specific f and g are close related to the above general form given by ADMM. The operator $\mathbf{prox}_\psi(\cdot)$ has nice properties as reviewed in Proposition 1, which enables the possibility of NN-based approximation even when f and g are not differentiable. One noted example is the LEC case when $g(\mathbf{H}_e) = \langle \mathbf{y}, \varsigma(\mathbf{H}_e) \rangle^p$.

Proposition 1 ([64, 65]). *If $\psi(\cdot) : \mathbb{R}^K \rightarrow \mathbb{R}$ is a lower semi-continuous convex function, then $\mathbf{prox}_\psi(\cdot)$ is 1-Lipschitz continuous.*

The node-side operations, gradient $\nabla f(\cdot; \mathbf{x}_v)$ and proximal gradient $\mathbf{prox}_{\eta f(\cdot; \mathbf{x}_v)}(\cdot)$ are relatively easy to model, while the operations on hyperedges are more complicated. We name gradient $\nabla g(\cdot) : \mathbb{R}^{|e|} \rightarrow \mathbb{R}^{|e|}$ and proximal gradient $\mathbf{prox}_{\eta g}(\cdot) : \mathbb{R}^{|e|} \rightarrow \mathbb{R}^{|e|}$ as *hyperedge diffusion operators*, since they summarize the collection of node features inside a hyperedge and dispatch the aggregated information to interior nodes individually. Next, we reveal one crucial property of those hyperedge diffusion operators by the following proposition (see the proof in Appendix B.1):

Proposition 2. *Given any permutation-invariant hyperedge potential function $g(\cdot)$, hyperedge diffusion operators $\mathbf{prox}_{\eta g}(\cdot)$ and $\nabla g(\cdot)$ are permutation equivariant.*

It states that an permutation invariant hyperedge potential leads to an operator that should process different nodes in a permutation-equivariant way.

3.2 Building Equivariant Hyperedge Diffusion Operators

To model permutation-equivariant diffusion operators, we may resort to previous studies on NN architectures to represent equivariant multi-set functions [50–52]. However, there are still some gaps when we apply their approaches in the hypergraph setting. In practice, these works focus on the

Algorithm 1: ED-HNN

Initialization: $H^{(0)} = X$ and three MLPs $\hat{\phi}, \hat{\rho}, \hat{\psi}$ (shared across L layers).

For $t = 0, 1, 2, \dots, L - 1$, **do:**

1. Designing the messages from \mathcal{V} to \mathcal{E} : $\mathbf{m}_{u \rightarrow e}^{(t)} = \hat{\phi}(\mathbf{h}_u^{(t)})$, for all $u \in \mathcal{V}$.
 2. Sum $\mathcal{V} \rightarrow \mathcal{E}$ messages over hyperedges $\mathbf{m}_e^{(t)} = \sum_{u \in e} \mathbf{m}_{u \rightarrow e}^{(t)}$, for all $e \in \mathcal{E}$.
 3. Broadcast $\mathbf{m}_e^{(t)}$ and design the messages from \mathcal{E} to \mathcal{V} : $\mathbf{m}_{e \rightarrow v}^{(t)} = \hat{\rho}(\mathbf{h}_v^{(t)}, \mathbf{m}_e^{(t)})$, for all $v \in e$.
 4. Update $\mathbf{h}_v^{(t+1)} = \hat{\psi}(\mathbf{h}_v^{(t)}, \sum_{e: u \in e} \mathbf{m}_{e \rightarrow u}^{(t)}, \mathbf{x}_v, d_v)$, for all $v \in \mathcal{V}$.
-

case with separate multi-sets, such as prediction over separate collections of images or 3-D points, while hypergraphs contain a large number of coupled hyperedges. As hyperedges could be large and irregular in practice, how to build scalable equivariant NN architectures on hyperedges is challenging. Note that although graphs also couple many edges, edges in graphs are of regular size two. Building equivariant edge operation in graphs is often much less crucial or challenging.

Our design is built upon the following Theorem 1. We leave the proof in Appendix B.2.

Theorem 1. $\psi(\cdot) : [0, 1]^K \rightarrow \mathbb{R}^K$ is a continuous permutation-equivariant function, if and only if it can be represented as $[\psi(\mathbf{Z})]_i = \rho(\mathbf{z}_i, \sum_{j=1}^K \phi(\mathbf{z}_j))$, $i \in [K]$ for any $\mathbf{Z} = [\dots, \mathbf{z}_i, \dots]^\top \in [0, 1]^K$, where $\rho : \mathbb{R}^{K'} \rightarrow \mathbb{R}$, $\phi : \mathbb{R} \rightarrow \mathbb{R}^{K'-1}$ are two continuous functions, and K' could be as small as K .

Theorem 1 indicates that any continuous permutation-equivariant function is a composition of a continuous function ρ and the sum of another continuous function ϕ on each input entry. This result generalizes the representation of permutation-invariant functions by $\rho(\sum_{i=1}^K \phi(\mathbf{z}_i))$ in [50] to the equivariant case. An architecture with a similar spirit was proposed in [52] for equivariant set function representations. However, in practice, the work targeted at a single set representation instead of hypergraph with coupled sets [52]. In theory, their proof used the universality of equivariant polynomials as a bridge so their construction $\hat{\psi}(\mathbf{Z})$ only allows approximation, i.e., small $\|\psi(\mathbf{Z}) - \hat{\psi}(\mathbf{Z})\|$ instead of precise representation in Theorem 1. Also, $K' \geq K$ is tight by generalizing the proof for invariant set function representation [66]. Note that, in practice, ρ and ϕ often need to be further approximated by NNs. So, the precise representation in Theorem 1 has more value of its theoretical implication than its practical usage given the results in [52].

The above theoretical observation inspires the design of equivariant hyperedge diffusion operators. Specifically, for an operator $\hat{\psi}(\cdot) : \mathbb{R}^{|e|} \rightarrow \mathbb{R}^{|e|}$ that may denote either gradient $\nabla g(\cdot)$ or proximal gradient $\text{prox}_{ng}(\cdot)$ for each hyperedge e , we may parameterize it as:

$$[\hat{\psi}(\mathbf{H}_e)]_v = \hat{\rho}(\mathbf{h}_v, \sum_{u \in e} \hat{\phi}(\mathbf{h}_u)), \text{ for } v \in e, \text{ where } \hat{\rho}, \hat{\phi} \text{ are multi-layer perceptions (MLPs)}. \quad (5)$$

Intuitively, the inner sum collects the $\hat{\phi}$ -encoding node features within a hyperedge and then $\hat{\rho}$ combines the collection with the features from each node further to perform separate operation.

The implementation of the above $\hat{\psi}$ is not trivial. A naive implementation is to generate an auxillary node to representation each (v, e) -pair for $v \in \mathcal{V}$ and $e \in \mathcal{E}$ and learn its representation as adopted in [28–30]. However, this may substantially increase the model complexity.

Our implementation is built upon the widely-used bipartite representations [24–26] (or star expansion [47,48], equivalently) of hypergraphs paired with the standard message passing NN (MPNN) [49] that can be efficiently implemented via the commonly-used GNN platforms [45,46]. Specifically, we build a bipartite graph $\bar{\mathcal{G}} = (\bar{\mathcal{V}}, \bar{\mathcal{E}})$. The node set $\bar{\mathcal{V}}$ contains two parts $\mathcal{V} \cup \mathcal{V}_{\mathcal{E}}$ where \mathcal{V} is the original node set while $\mathcal{V}_{\mathcal{E}}$ contains nodes corresponding to original hyperedges $e \in \mathcal{E}$. Then, add an edge between $v \in \mathcal{V}$ and $e \in \mathcal{E}$ if $v \in e$. The model **ED-HNN** is implemented by following **Algorithm 1**.

The equivariant diffusion operator $\hat{\psi}$ can be constructed via steps 1-3. The last step is to update the node features to accomplish the first two terms in Eq. 2 or the ADMM update Eq. 4. The initial attributes \mathbf{x}_v and node degrees are included to match the diffusion algorithm by design. As the diffusion operators are shared across iterations, ED-HNN shares parameters across layers. Now, we summarize the joint contribution of our theory and efficient implementation as follows.

Proposition 3. *MPNNs on bipartite representations (or star expansions) of hypergraphs are expressive enough to learn any continuous diffusion operators induced by invariant hyperedge potentials.*

ED-HNN can well approximate the GD algorithm (Eq. 2), while ED-HNN does not perfectly match ADMM unless we assume $\mathbf{Q}_e^{(t)} = \mathbf{H}_e^{(t)}$ in Eq. 3 for a practical consideration. This assumption may reduce the performance of the hypergraph diffusion algorithm while our model ED-HNN has already achieved good enough empirical performance. Tracking $\mathbf{Q}_e^{(t)}$ means recording the messages from \mathcal{E} to \mathcal{V} for every iteration, which is not supported by the current GNN platforms [45, 46] and may consume more memory. We leave the study that can represent $\mathbf{Q}_e^{(t)}$ as a future study. A co-design of the algorithm and the system may be needed.

Extension. Our ED-HNN can be naturally extended to build equivariant node operators because of the duality between hyperedges and nodes, though this is not necessary in the traditional hypergraph diffusion problem Eq. 1. Specifically, we call this model ED-HNNII, which simply revises the step 1 in ED-HNN as $\mathbf{m}_{u \rightarrow e}^{(t)} = \hat{\phi}(\mathbf{h}_u^{(t)}, \mathbf{m}_e^{(t-1)})$ for any e such that $u \in e$. Due to the page limit, we put some experiment results on ED-HNNII in Appendix C.1.

3.3 Discussion: Advantages of ED-HNN in Heterophilic Settings and Deep Models

Here, we discuss several advantages of ED-HNN due to the design of equivariant diffusion operators.

Heterophily describes the network phenomenon where nodes with the same labels and attributes are less likely to connect to each other directly [67]. Predicting node labels in heterophilic networks is known to be more challenging than that in homophilic networks, and thus has recently become an important research direction in the community [68–71]. Heterophily has been proved as a more common phenomenon in hypergraphs than in graphs since it is hard to expect that all nodes in a giant hyperedge share a common label [16, 72]. Moreover, predicting node labels in heterophilic hypergraphs is more challenging than that in graphs as a hyperedge may consist of the nodes from multiple categories.

Learnable equivariant diffusion operators are expected to be superior in predicting heterophilic node labels. For example, if a hyperedge e of size 3 is known to cover two nodes v, u from class \mathcal{C}_1 while one node w from class \mathcal{C}_0 . We may use the LEC potential $\langle \mathbf{y}, \varsigma(\mathbf{H}_e) \rangle^2$ by setting $\mathbf{y} = [1, -1, 0]^\top$. Suppose the three nodes’ attributes are $\mathbf{H}_e = [\mathbf{h}_v, \mathbf{h}_u, \mathbf{h}_w]^\top = [0.7, 0.5, 0.3]^\top$, where $\mathbf{h}_v, \mathbf{h}_u$ are close as they are from the same class. One may check the hyperedge diffusion operator gives $\nabla g(\mathbf{H}_e) = [0.4, -0.4, 0]^\top$. One-step gradient descent $\mathbf{h}_v - \eta[\nabla g(\mathbf{H}_e)]_v$ with a proper step size ($\eta < 0.5$) drags \mathbf{h}_v and \mathbf{h}_u closer while keeping \mathbf{h}_w unchanged. However, invariant diffusion that allocates every node with the same change does not help with the classification. If the ground truth is different, say w, u from the same class and v from the other, using the above \mathbf{y} may increase the error. However, learnable operators can solve the problem, e.g., by learning another $\mathbf{y} = [0, 1, -1]^\top$.

Moreover, equivariant hyperedge diffusion operators are also good at building deep models. GNNs tend to degenerate the performance when going deep, which is often attributed to their oversmoothing [73, 74] and overfitting problems [75]. Equivariant operators allocating different messages to different nodes helps with overcoming the oversmoothing issue. On the other hand, diffusion operators by sharing parameters across different layers may reduce the risk of overfitting.

3.4 Previous Hypergraph Neural Networks for Representing Hypergraph Diffusion

ED-HNN is the first HNN inspired by the general class of hypergraph diffusion and can provably achieve universal approximation of hyperedge diffusion operators. So, how about previous HNNs representing hypergraph diffusion? We temporarily ignore the big difference in whether parameters are shared across layers and give analysis as follows. HGNN [22] runs graph convolution [76] on clique expansions of hypergraphs, which directly assumes the hyperedge potentials follow CE plus pairwise potentials and cannot learn other operations on hyperedges. HyperGCN [23] essentially leverages the total variation potential by adding mediator nodes to each hyperedge, which adopts a transformation technique in [77, 78]. A few works view hyperedges as multi-sets of nodes and nodes as multi-sets of hyperedges [24–30, 79]. Among them, HNNH [24], UniGNNs [25], EHGNN [79] and AllSet [26] build two invariant set-pooling functions on both the hyperedge and node sides, which cannot represent equivariant functions. One subtle point is that Uni{GIN, GraphSAGE, GCNII} [25] adopt jump link to pass node features from the former layer to the next and may expect to use a complicated node-side invariant function $\hat{\psi}'(\mathbf{h}_v^{(t)}, \sum_{e: v \in e} \mathbf{m}_e^{(t)})$ to

Table 1: Dataset statistics. CE homophily is the homophily score [68] based on CE of hypergraphs.

	Cora	Citeseer	Pubmed	Cora-CA	DBLP-CA	Congress	Senate	Walmart	House
# nodes	2708	3312	19717	2708	41302	1718	282	88860	1290
# edges	1579	1079	7963	1072	22363	83105	315	69906	340
# classes	7	6	3	7	6	2	2	11	2
avg. $ e $	1.748	1.541	1.963	1.929	2.213	8.654	9.531	3.461	8.056
CE Homophily	0.897	0.893	0.952	0.803	0.869	0.555	0.498	0.530	0.509

approximate our $\hat{\psi}(\mathbf{h}_v^{(t)}, \sum_{e:v \in e} \mathbf{m}_{e \rightarrow v}^{(t)}) = \hat{\psi}(\mathbf{h}_v^{(t)}, \sum_{e:v \in e} \hat{\rho}(\mathbf{h}_v^{(t)}, \mathbf{m}_e^{(t)}))$ in Step 4 of **Algorithm 1** directly. This may be doable in theory. However, the jump-link solution may expect to have a higher dimension of $\mathbf{m}_e^{(t)}$ ($\text{dim} = |\cup_{e:v \in e} e|$) so that the sum pooling $\sum_{e:v \in e} \mathbf{m}_e^{(t)}$ does not lose anything from the neighboring nodes of v before interacting with $\mathbf{h}_v^{(t)}$, while in ED-HNN, $\mathbf{m}_e^{(t)}$ needs $\text{dim} = |e|$ according to Theorem 1. Our empirical experiments also verify more expressiveness of ED-HNN. HCHA [27] and UniGAT [30] compute attention weights as a result of combining node features and hyperedge messages, which looks like our ρ operation. However, a scalar attention weight is too limited to represent the potentially complicated ρ . HyperSAGE [28], MPNN-R [29] and LEGCN [30] may learn hyperedge equivariant operators, while they need many auxiliary nodes that represent node-hyperedge pairs. Of course, none of these works have mentioned any theoretical arguments on universal representation of hypergraph diffusion as ours.

4 Further Discussion on Related Works

We have discussed the most relevant works on HNN architectures and hypergraph diffusion algorithms in Sec. 3. Here, we review some relevant works on optimization-inspired NNs. Optimization-inspired NNs often get praised for their interpretability [80, 81] and certified convergence under certain conditions of the learned operators [82–84]. Early works that adopt optimization-inspired NNs focus on the applications such as compressive sensing [85–88], speech processing [89, 90], image denoising [91–94], partitioning [95, 96], deblurring [97, 98] and so on. Recently, optimization-inspired NNs have also been applied to graphs [99–102]. They unroll either learnable [99, 101], fixed ℓ_1 -norm [100] or fixed ℓ_2 -norm pair-wise potentials [102] to formulate GNNs. Some works also view the graph diffusion as an ODE [103, 104], which essentially corresponds to our gradient descent Eq. 2. As there are only pairwise relations in graphs, the GNN design is often much simpler than the HNN counterpart. Neither expressivity nor equivariance has been investigated in these works. Implicit NNs [105, 106] are to directly parameterize the optimum of an optimization problem. Implicit NNs have also been applied to graphs [107–110] but not to hypergraphs. So, a future study of this work is to develop implicit models that can directly parameterize the solution to Eq. 1.

5 Experiments

5.1 Results on Benchmarking Datasets

Experiment Setting. In this subsection, we evaluate ED-HNN on nine real-world benchmarking hypergraphs. We focus on the semi-supervised node classification task. The nine datasets include co-citation networks (Cora, Citeseer, Pubmed), co-authorship networks (Cora-CA, DBLP-CA) [23], Walmart [111], House [112], Congress and Senate [113, 114]. More details of these datasets can be found in Appendix C.2. Since the last four hypergraphs do not contain node attributes, we follow the method of [26] to generate node features from label-dependent Gaussian distribution [115].

As we show in Table 1, these datasets already cover sufficiently diverse hypergraphs in terms of scale, structure, and homo-/heterophily. We compare our method with top-performing models on these benchmarks, including HGNN [22], HCHA [27], HNHN [24], HyperGCN [23], UniGCNII [25], AllDeepSets [26], and AllSetTransformer [26]. All the hyperparameters for baselines follow from [26] and we fix the learning rate, weight decay and other training recipes same with the baselines. Other model specific hyperparameters are obtained via grid search (see Appendix C.3). We randomly split the data into training/validation/test samples using 50%/25%/25% splitting percentage by following [26]. We choose prediction accuracy as the evaluation metric. We run each model for ten times with different training/validation splits to obtain the standard deviation.

Performance Analysis. Table 2 shows the results. Our ED-HNN uniformly outperforms all the compared models on all the datasets. We observe that the top-performing baseline models are AllSetTransformer, AllDeepSets and UniGCNII. As having been analyzed in Sec. 3.4, they model

Table 2: Prediction Accuracy (%). **Bold font**[†] highlights when ED-HNN significantly (difference in means $> 0.5 \times \text{std}$) outperforms all baselines. The best baselines are underlined. The training and testing times are test on Walmart by using the same server with one GPU NVIDIA RTX A6000.

	Cora	Citeseer	Pubmed	Cora-CA	DBLP-CA	Training Time (10^{-1} s)
HGNN [25]	79.39 \pm 1.36	72.45 \pm 1.16	86.44 \pm 0.44	82.64 \pm 1.65	91.03 \pm 0.20	0.24 \pm 0.51
HCHA [27]	79.14 \pm 1.02	72.42 \pm 1.42	86.41 \pm 0.36	82.55 \pm 0.97	90.92 \pm 0.22	0.24 \pm 0.01
HNHN [24]	76.36 \pm 1.92	72.64 \pm 1.57	86.90 \pm 0.30	77.19 \pm 1.49	86.78 \pm 0.29	0.30 \pm 0.56
HyperGCN [23]	78.45 \pm 1.26	71.28 \pm 0.82	82.84 \pm 8.67	79.48 \pm 2.08	89.38 \pm 0.25	0.42 \pm 1.51
UniGCNII [25]	78.81 \pm 1.05	73.05 \pm 2.21	88.25 \pm 0.40	83.60 \pm 1.14	91.69 \pm 0.19	4.36 \pm 1.18
AllDeepSets [26]	76.88 \pm 1.80	70.83 \pm 1.63	<u>88.75 \pm 0.33</u>	<u>81.97 \pm 1.50</u>	<u>91.27 \pm 0.27</u>	1.23 \pm 1.09
AllSetTransformer [26]	78.58 \pm 1.47	73.08 \pm 1.20	88.72 \pm 0.37	83.63 \pm 1.47	91.53 \pm 0.23	1.64 \pm 1.63
ED-HNN (ours)	80.31 \pm 1.35[†]	73.70 \pm 1.38[†]	89.03 \pm 0.53[†]	83.97 \pm 1.55	91.90 \pm 0.19[†]	1.71 \pm 1.13
	Congress	Senate	Walmart	House	Avg. Rank	Inference Time (10^{-2} s)
HGNN [25]	91.26 \pm 1.15	48.59 \pm 4.52	62.00 \pm 0.24	61.39 \pm 2.96	4.89	1.01 \pm 0.04
HCHA [27]	90.43 \pm 1.20	48.62 \pm 4.41	62.35 \pm 0.26	61.36 \pm 2.53	5.44	1.54 \pm 0.18
HNHN [24]	53.35 \pm 1.45	50.93 \pm 6.33	47.18 \pm 0.35	67.80 \pm 2.59	7.11	6.11 \pm 0.05
HyperGCN [23]	55.12 \pm 1.96	42.45 \pm 3.67	44.74 \pm 2.81	48.32 \pm 2.93	7.33	0.87 \pm 0.06
UniGCNII [25]	<u>94.81 \pm 0.81</u>	49.30 \pm 4.25	54.45 \pm 0.37	67.25 \pm 2.57	3.67	21.22 \pm 0.13
AllDeepSets [26]	91.80 \pm 1.53	48.17 \pm 5.67	64.55 \pm 0.33	67.82 \pm 2.40	4.89	5.35 \pm 0.33
AllSetTransformer [26]	92.16 \pm 1.05	<u>51.83 \pm 5.22</u>	<u>65.46 \pm 0.25</u>	<u>69.33 \pm 2.20</u>	2.67	6.06 \pm 0.67
ED-HNN (ours)	95.00 \pm 0.99	64.79 \pm 5.14[†]	66.91 \pm 0.41[†]	72.45 \pm 2.28[†]	1.00	5.87 \pm 0.36

Table 3: Prediction Accuracy (%) over Synthetic Hypergraphs with Controlled Heterophily α .

	Homophily			Heterophily		
	$\alpha = 1$	$\alpha = 2$	$\alpha = 3$	$\alpha = 4$	$\alpha = 6$	$\alpha = 7$
HGNN [25]	99.86 \pm 0.05	90.42 \pm 1.14	66.60 \pm 1.60	57.90 \pm 1.43	50.77 \pm 1.94	48.68 \pm 1.21
HGNN + JumpLink [25]	99.29 \pm 0.19	92.61 \pm 0.97	79.59 \pm 2.32	64.39 \pm 1.55	55.39 \pm 2.01	51.14 \pm 2.05
AllDeepSets [26]	99.86 \pm 0.07	99.13 \pm 0.31	92.39 \pm 1.68	80.12 \pm 2.31	56.42 \pm 0.85	52.14 \pm 2.88
AllDeepSets + JumpLink [25]	99.95 \pm 0.07	99.08 \pm 0.24	93.52 \pm 1.31	83.45 \pm 2.64	59.68 \pm 1.27	52.21 \pm 2.36
AllSetTransformer [26]	98.60 \pm 0.48	95.89 \pm 0.90	88.38 \pm 1.81	83.34 \pm 1.33	54.13 \pm 4.83	50.15 \pm 1.73
ED-HNN (ours)	99.95 \pm 0.08	99.68 \pm 0.13[†]	95.37 \pm 1.23[†]	90.35 \pm 0.83[†]	65.58 \pm 0.76[†]	54.31 \pm 2.40[†]

invariant set functions on both node and hyperedge sides. UniGCNII also adds initial and jump links, which accidentally resonates with our design principle (the step 4 in Algorithm 1). However, their performance has large variation across different datasets. For example, UniGCNII attains promising performance on citation networks, however, has subpar results on Walmart dataset. In contrast, our model achieves stably superior results, surpassing AllSet models by 12.9% on Senate and UniGCNII by 12.5% on Walmart. We owe our empirical significance to the theoretical design of exact equivariant function representation. Regarding the computational efficiency, we report the wall-clock times for training (for 100 epochs) and testing of all models over the largest hypergraph Walmart, where all models use the same hyperparameters that achieve the reported performance on the left. Our model achieves efficiency comparable to AllSet models [26] and is much faster than UniGCNII. So, the implementation of equivariant computation in ED-HNN is still efficient.

5.2 Results on Synthetic Heterophilic Hypergraph Dataset

Experiment Setting. As discussed, ED-HNN is expected to perform well on heterophilic hypergraphs. We evaluate this point by using synthetic datasets with controlled heterophily. We generate data by using contextual hypergraph stochastic block model [115–117]. Specifically, we draw two classes of 2, 500 nodes each and then randomly sample 1,000 hyperedges. Each hyperedge consists of 15 nodes, among which α_i many are sampled from class i . We use $\alpha = \min\{\alpha_1, \alpha_2\}$ to denote the heterophily level. Afterwards, we generate label-dependent Gaussian node features. We test both homophilic ($\alpha = 1, 2$ or CE homophily ≥ 0.7) and heterophilic ($\alpha = 4 \sim 7$ or CE homophily ≤ 0.7) cases. We compare ED-HNN with HGNN [22], AllSet models [26] and their variants with jump links. We follow previous 50%/25%/25% data splitting methods and repeated 10 times the experiment.

Results. Table 3 shows the results. On homophilic datasets, all the models can achieve good results, while ED-HNN keeps slightly better than others. Once α surpasses 3, i.e., entering the heterophilic regime, the superiority of ED-HNN is more obvious. The jump-link trick indeed also helps, while building equivariance as ED-HNN does directly provides more significant improvement.

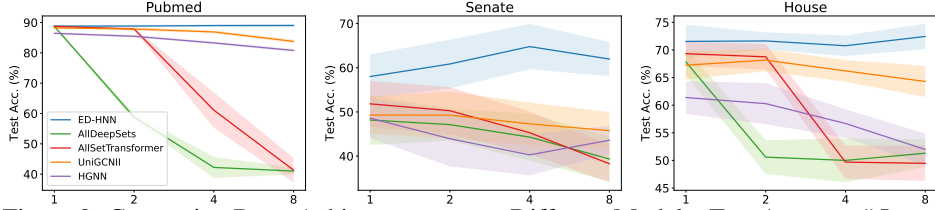


Figure 2: Comparing Deep Architectures across Different Models: Test Acc. v.s. # Layers

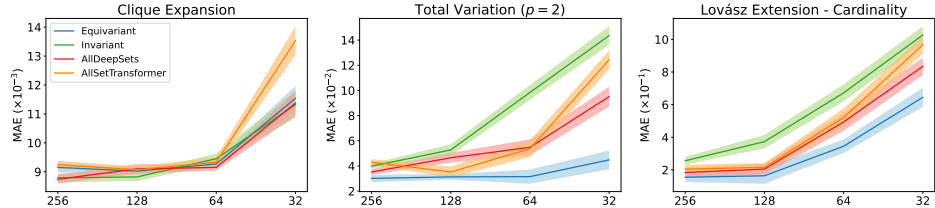


Figure 3: Comparing the Powers to Represent known Diffusion: MAE v.s. Latent Dimensions

5.3 Benefits in Deepening Hypergraph Neural Networks

We also demonstrate that by using diffusion models and parameter tying, ED-HNN can benefit from deeper architectures, while other HNNs cannot. Fig. 2 illustrates the performance of different models versus the number of network layers. We compare with HGNN [22], AllSet models [26], and UniGCNII [25]. UniGCNII inherits from [118] which is known to be effective to counteract oversmoothness. The results reveal that AllSet models suffer from going deep. HGNN working through more lightweight mechanism has better tolerance to depth. However, none of them can benefit from deepening. On the contrary, ED-HNN successfully leverages deeper architecture to achieve higher accuracy. For example, adding more layers boosts ED-HNN by $\sim 1\%$ in accuracy on Pubmed and House, while elevating ED-HNN from 58.01% to 64.79% on Senate dataset.

5.4 Expressiveness Justification on the Synthetic Diffusion Dataset

We are to evaluate the ability of ED-HNN to express given hypergraph diffusion. We generate semi-synthetic diffusion data using the Senate hypergraph [112] and synthetic node features. The data consists of 1,000 pairs $(\mathbf{H}^{(0)}, \mathbf{H}^{(1)})$. The initial node features $\mathbf{H}^{(0)}$ are sampled from 1-dim Gaussian distributions. To obtain $\mathbf{H}^{(1)}$ we apply the gradient step in Eq. 2. For non-differential cases, we adopt subgradients for convenient computation. We fix node potentials as $f(\mathbf{h}_v; \mathbf{x}_v) = (\mathbf{h}_v - \mathbf{x}_v)^2$ and consider 3 different edge potentials in Example 1 with varying complexities: a) CE, b) TV ($p=2$) and c) LEC. The goal is to let one-layer models $\mathcal{V} \rightarrow \mathcal{E} \rightarrow \mathcal{V}$ to recover $\mathbf{H}^{(1)}$. We compare ED-HNN with our implemented baseline (Invariant) with parameterized invariant set functions on both the node and hyperedge sides, and AllSet models [26] that also adopt invariant set functions. We keep the scale of all models almost the same to give fair comparison, of which more details are given in Appendix C.5. The results are reported in Fig. 3. The CE case gives invariant diffusion so all models can learn it well. The TV case mostly shows the benefit of the equivariant architecture, where the error almost does not increase even when the dimension decreases to 32. The LEC case is challenging for all models, though ED-HNN is still the best. The reason, we think, is that learning the sorting operation in LEC via the sum pooling in Eq. 5 is empirically challenging albeit theoretically doable. A similar phenomenon has been observed in previous literatures [66, 119].

6 Conclusion

This work introduces a new hypergraph neural network ED-HNN that can model hypergraph diffusion process. We show that any hypergraph diffusion with permutation-invariant potential functions can be represented by iterating equivariant diffusion operators. ED-HNN provides an efficient way to model such operators based on the commonly-used GNN platforms. ED-HNN shows superiority in processing heterophilic hypergraphs and constructing deep models. In the future, we would like to apply ED-HNN to other tasks such as hypergraph regression tasks and develop implicit HNNs that can directly optimize the optima of hypergraph diffusion problems.

References

- [1] X. Zhu, *Semi-supervised learning with graphs*. Carnegie Mellon University, 2005.
- [2] X. Zhu, Z. Ghahramani, and J. D. Lafferty, “Semi-supervised learning using gaussian fields and harmonic functions,” in *International Conference on Machine Learning (ICML)*, 2003.
- [3] D. Zhou, O. Bousquet, T. N. Lal, J. Weston, and B. Schölkopf, “Learning with local and global consistency,” in *Advances in Neural Information Processing Systems (NeurIPS)*, 2004.
- [4] W. L. Hamilton, “Graph representation learning,” 2020.
- [5] M. Nickel, K. Murphy, V. Tresp, and E. Gabrilovich, “A review of relational machine learning for knowledge graphs,” *Proceedings of the IEEE*, 2015.
- [6] I. Chami, S. Abu-El-Haija, B. Perozzi, C. Ré, and K. Murphy, “Machine learning on graphs: A model and comprehensive taxonomy,” *arXiv preprint arXiv:2005.03675*, 2020.
- [7] A. R. Benson, D. F. Gleich, and D. J. Higham, “Higher-order network analysis takes off, fueled by classical ideas and new data,” *arXiv preprint arXiv:2103.05031*, 2021.
- [8] M. T. Schaub, Y. Zhu, J.-B. Seby, T. M. Roddenberry, and S. Segarra, “Signal processing on higher-order networks: Livin’ on the edge... and beyond,” *Signal Processing*, 2021.
- [9] F. Battiston, G. Cencetti, I. Iacopini, V. Latora, M. Lucas, A. Patania, J.-G. Young, and G. Petri, “Networks beyond pairwise interactions: structure and dynamics,” *Physics Reports*, 2020.
- [10] R. Lambiotte, M. Rosvall, and I. Scholtes, “From networks to optimal higher-order models of complex systems,” *Nature physics*, 2019.
- [11] Y. Liu, J. Ma, and P. Li, “Neural predicting higher-order patterns in temporal networks,” in *Proceedings of the ACM Web Conference 2022*, 2022, pp. 1340–1351.
- [12] S. Mangan and U. Alon, “Structure and function of the feed-forward loop network motif,” *National Academy of Sciences*, 2003.
- [13] A. R. Benson, D. F. Gleich, and J. Leskovec, “Higher-order organization of complex networks,” *Science*, 2016.
- [14] C. E. Tsourakakis, J. Pachocki, and M. Mitzenmacher, “Scalable motif-aware graph clustering,” in *Proceedings of the Web Conference*, 2017, pp. 1451–1460.
- [15] P. Li, H. Dau, G. Puleo, and O. Milenkovic, “Motif clustering and overlapping clustering for social network analysis,” in *INFOCOM 2017-IEEE Conference on Computer Communications, IEEE*. IEEE, 2017, pp. 1–9.
- [16] P. Li and O. Milenkovic, “Inhomogeneous hypergraph clustering with applications,” in *Advances in Neural Information Processing Systems*, 2017, pp. 2305–2315.
- [17] X. Xia, H. Yin, J. Yu, Q. Wang, L. Cui, and X. Zhang, “Self-supervised hypergraph convolutional networks for session-based recommendation,” in *Proceedings of the AAAI Conference on Artificial Intelligence*, vol. 35, no. 5, 2021, pp. 4503–4511.
- [18] J. Wang, K. Ding, Z. Zhu, and J. Caverlee, “Session-based recommendation with hypergraph attention networks,” in *Proceedings of the 2021 SIAM International Conference on Data Mining (SDM)*. SIAM, 2021, pp. 82–90.
- [19] J. Wang, K. Ding, L. Hong, H. Liu, and J. Caverlee, “Next-item recommendation with sequential hypergraphs,” in *Proceedings of the 43rd international ACM SIGIR conference on research and development in information retrieval*, 2020, pp. 1101–1110.
- [20] N. Wang, S. Wang, Y. Wang, Q. Z. Sheng, and M. A. Orgun, “Exploiting intra-and inter-session dependencies for session-based recommendations,” *World Wide Web*, vol. 25, no. 1, pp. 425–443, 2022.
- [21] C. Berge, *Hypergraphs: combinatorics of finite sets*. Elsevier, 1984, vol. 45.
- [22] Y. Feng, H. You, Z. Zhang, R. Ji, and Y. Gao, “Hypergraph neural networks,” in *Proceedings of the AAAI Conference on Artificial Intelligence*, vol. 33, no. 01, 2019, pp. 3558–3565.
- [23] N. Yadati, M. Nimishakavi, P. Yadav, V. Nitin, A. Louis, and P. Talukdar, “Hypergcn: A new method for training graph convolutional networks on hypergraphs,” *Advances in neural information processing systems*, vol. 32, 2019.

- [24] Y. Dong, W. Sawin, and Y. Bengio, “Hnhn: Hypergraph networks with hyperedge neurons,” *arXiv preprint arXiv:2006.12278*, 2020.
- [25] J. Huang and J. Yang, “Unignn: a unified framework for graph and hypergraph neural networks,” *arXiv preprint arXiv:2105.00956*, 2021.
- [26] E. Chien, C. Pan, J. Peng, and O. Milenkovic, “You are allset: A multiset function framework for hypergraph neural networks,” in *International Conference on Learning Representations*, 2022.
- [27] S. Bai, F. Zhang, and P. H. Torr, “Hypergraph convolution and hypergraph attention,” *Pattern Recognition*, vol. 110, p. 107637, 2021.
- [28] D. Arya, D. K. Gupta, S. Rudinac, and M. Worring, “Hypersage: Generalizing inductive representation learning on hypergraphs,” *arXiv preprint arXiv:2010.04558*, 2020.
- [29] N. Yadati, “Neural message passing for multi-relational ordered and recursive hypergraphs,” *Advances in Neural Information Processing Systems*, vol. 33, pp. 3275–3289, 2020.
- [30] C. Yang, R. Wang, S. Yao, and T. Abdelzaher, “Hypergraph learning with line expansion,” *arXiv preprint arXiv:2005.04843*, 2020.
- [31] D. Zhou, J. Huang, and B. Schölkopf, “Learning with hypergraphs: Clustering, classification, and embedding,” in *Advances in Neural Information Processing Systems*, 2007, pp. 1601–1608.
- [32] M. Hein, S. Setzer, L. Jost, and S. S. Rangapuram, “The total variation on hypergraphs-learning on hypergraphs revisited,” in *Advances in Neural Information Processing Systems*, 2013, pp. 2427–2435.
- [33] P. Li, N. He, and O. Milenkovic, “Quadratic decomposable submodular function minimization: Theory and practice.” *Journal of Machine Learning Research (JMLR)*, 2020.
- [34] M. Liu, N. Veldt, H. Song, P. Li, and D. F. Gleich, “Strongly local hypergraph diffusions for clustering and semi-supervised learning,” in *Proceedings of the Web Conference 2021*, 2021, pp. 2092–2103.
- [35] K. Fountoulakis, P. Li, and S. Yang, “Local hyper-flow diffusion,” *Advances in Neural Information Processing Systems*, vol. 34, 2021.
- [36] Y. Takai, A. Miyauchi, M. Ikeda, and Y. Yoshida, “Hypergraph clustering based on pagerank,” in *Proceedings of the 26th ACM SIGKDD International Conference on Knowledge Discovery & Data Mining*, 2020, pp. 1970–1978.
- [37] C. Zhang, S. Hu, Z. G. Tang, and T. H. Chan, “Re-revisiting learning on hypergraphs: confidence interval and subgradient method,” in *International Conference on Machine Learning*, 2017, pp. 4026–4034.
- [38] F. Tudisco, A. R. Benson, and K. Prokopchik, “Nonlinear higher-order label spreading,” in *Proceedings of the Web Conference*, 2021.
- [39] P. Li and O. Milenkovic, “Submodular hypergraphs: p-laplacians, cheeger inequalities and spectral clustering,” in *International Conference on Machine Learning (ICML)*, 2018.
- [40] P. Li, N. He, and O. Milenkovic, “Quadratic decomposable submodular function minimization,” in *Advances in Neural Information Processing Systems (NeurIPS)*, 2018.
- [41] U. Chitra and B. Raphael, “Random walks on hypergraphs with edge-dependent vertex weights,” in *International Conference on Machine Learning (ICML)*, 2019.
- [42] S. Zhang, Z. Ding, and S. Cui, “Introducing hypergraph signal processing: Theoretical foundation and practical applications,” *IEEE Internet of Things Journal*, 2019.
- [43] N. Komodakis and N. Paragios, “Beyond pairwise energies: Efficient optimization for higher-order mrfs,” in *IEEE Conference on Computer Vision and Pattern Recognition (CVPR)*, 2009.
- [44] T. Werner, “High-arity interactions, polyhedral relaxations, and cutting plane algorithm for soft constraint optimisation (map-mrf),” in *IEEE Conference on Computer Vision and Pattern Recognition (CVPR)*, 2008.
- [45] M. Fey and J. E. Lenssen, “Fast graph representation learning with PyTorch Geometric,” in *International Conference on Learning Representations (ICLR) Workshop on Representation Learning on Graphs and Manifolds*, 2019.

- [46] M. Wang, D. Zheng, Z. Ye, Q. Gan, M. Li, X. Song, J. Zhou, C. Ma, L. Yu, Y. Gai, T. Xiao, T. He, G. Karypis, J. Li, and Z. Zhang, “Deep graph library: A graph-centric, highly-performant package for graph neural networks,” *arXiv preprint arXiv:1909.01315*, 2019.
- [47] S. Agarwal, K. Branson, and S. Belongie, “Higher order learning with graphs,” in *International Conference on Machine Learning (ICML)*, 2006.
- [48] J. Y. Zien, M. D. Schlag, and P. K. Chan, “Multilevel spectral hypergraph partitioning with arbitrary vertex sizes,” *IEEE Transactions on computer-aided design of integrated circuits and systems*, 1999.
- [49] J. Gilmer, S. S. Schoenholz, P. F. Riley, O. Vinyals, and G. E. Dahl, “Neural message passing for quantum chemistry,” in *International Conference on Machine Learning (ICML)*, 2017.
- [50] M. Zaheer, S. Kottur, S. Ravanbakhsh, B. Póczos, R. R. Salakhutdinov, and A. J. Smola, “Deep sets,” in *Advances in Neural Information Processing Systems (NeurIPS)*, 2017.
- [51] H. Maron, H. Ben-Hamu, N. Shamir, and Y. Lipman, “Invariant and equivariant graph networks,” in *International Conference on Learning Representations (ICLR)*, 2018.
- [52] N. Segol and Y. Lipman, “On universal equivariant set networks,” in *International Conference on Learning Representations (ICLR)*, 2020.
- [53] P. Stobbe and A. Krause, “Efficient minimization of decomposable submodular functions,” in *Advances in Neural Information Processing Systems (NeurIPS)*, 2010.
- [54] S. Jegelka, F. Bach, and S. Sra, “Reflection methods for user-friendly submodular optimization,” in *Advances in Neural Information Processing Systems (NeurIPS)*, 2013.
- [55] P. Li and O. Milenkovic, “Revisiting decomposable submodular function minimization with incidence relations,” in *Advances in Neural Information Processing Systems (NeurIPS)*, 2018.
- [56] F. Tudisco, K. Prokopcik, and A. R. Benson, “A nonlinear diffusion method for semi-supervised learning on hypergraphs,” *arXiv preprint arXiv:2103.14867*, 2021.
- [57] L. Lovász, “Submodular functions and convexity,” in *Mathematical Programming The State of the Art*, 1983.
- [58] N. Veldt, A. R. Benson, and J. Kleinberg, “Hypergraph cuts with general splitting functions,” *SIAM Review*, 2021.
- [59] I. E. Chien, H. Zhou, and P. Li, “ hs^2 : Active learning over hypergraphs with pointwise and pairwise queries,” in *International Conference on Artificial Intelligence and Statistics (AISTATS)*, 2019.
- [60] Y. Yoshida, “Cheeger inequalities for submodular transformations,” in *Proceedings of the Thirtieth Annual ACM-SIAM Symposium on Discrete Algorithms*. SIAM, 2019, pp. 2582–2601.
- [61] L. Neuhäuser, R. Lambiotte, and M. T. Schaub, “Consensus dynamics and opinion formation on hypergraphs,” in *Higher-Order Systems*, 2022.
- [62] L. Neuhäuser, M. T. Schaub, A. Mellor, and R. Lambiotte, “Opinion dynamics with multi-body interactions,” in *International Conference on Network Games, Control and Optimization*, 2021.
- [63] S. Boyd, N. Parikh, E. Chu, B. Peleato, J. Eckstein *et al.*, “Distributed optimization and statistical learning via the alternating direction method of multipliers,” *Foundations and Trends® in Machine learning*, 2011.
- [64] N. Parikh and S. Boyd, “Proximal algorithms,” *Foundations and Trends in optimization*, 2014.
- [65] N. G. Polson, J. G. Scott, and B. T. Willard, “Proximal algorithms in statistics and machine learning,” *Statistical Science*, 2015.
- [66] E. Wagstaff, F. Fuchs, M. Engelcke, I. Posner, and M. A. Osborne, “On the limitations of representing functions on sets,” in *International Conference on Machine Learning (ICML)*, 2019.
- [67] E. M. Rogers, *Diffusion of innovations*, 2010.
- [68] H. Pei, B. Wei, K. C.-C. Chang, Y. Lei, and B. Yang, “Geom-gcn: Geometric graph convolutional networks,” in *International Conference on Learning Representations (ICLR)*, 2020.

- [69] J. Zhu, Y. Yan, L. Zhao, M. Heimann, L. Akoglu, and D. Koutra, “Beyond homophily in graph neural networks: Current limitations and effective designs,” in *Advances in Neural Information Processing Systems (NeurIPS)*, 2020.
- [70] E. Chien, J. Peng, P. Li, and O. Milenkovic, “Adaptive universal generalized pagerank graph neural network,” in *International Conference on Learning Representations (ICLR)*, 2021.
- [71] D. Lim, F. Hohne, X. Li, S. L. Huang, V. Gupta, O. Bhalerao, and S. N. Lim, “Large scale learning on non-homophilous graphs: New benchmarks and strong simple methods,” in *Advances in Neural Information Processing Systems (NeurIPS)*, 2021.
- [72] N. Veldt, A. R. Benson, and J. Kleinberg, “Higher-order homophily is combinatorially impossible,” *SIAM Review (SIREV)*, 2022.
- [73] Q. Li, Z. Han, and X.-M. Wu, “Deeper insights into graph convolutional networks for semi-supervised learning,” in *AAAI conference on artificial intelligence (AAAI)*, 2018.
- [74] K. Oono and T. Suzuki, “Graph neural networks exponentially lose expressive power for node classification,” in *International Conference on Learning Representations (ICLR)*, 2019.
- [75] W. Cong, M. Ramezani, and M. Mahdavi, “On provable benefits of depth in training graph convolutional networks,” *Advances in Neural Information Processing Systems (NeurIPS)*, 2021.
- [76] T. N. Kipf and M. Welling, “Semi-supervised classification with graph convolutional networks,” in *International Conference on Learning Representations (ICLR)*, 2017.
- [77] T.-H. H. Chan, A. Louis, Z. G. Tang, and C. Zhang, “Spectral properties of hypergraph laplacian and approximation algorithms,” *Journal of the ACM (JACM)*, 2018.
- [78] T.-H. H. Chan and Z. Liang, “Generalizing the hypergraph laplacian via a diffusion process with mediators,” *Theoretical Computer Science*, 2020.
- [79] J. Jo, J. Baek, S. Lee, D. Kim, M. Kang, and S. J. Hwang, “Edge representation learning with hypergraphs,” in *Advances in Neural Information Processing Systems (NeurIPS)*, 2021.
- [80] V. Monga, Y. Li, and Y. C. Eldar, “Algorithm unrolling: Interpretable, efficient deep learning for signal and image processing,” *IEEE Signal Processing Magazine*, 2021.
- [81] T. Chen, X. Chen, W. Chen, H. Heaton, J. Liu, Z. Wang, and W. Yin, “Learning to optimize: A primer and a benchmark,” *arXiv preprint arXiv:2103.12828*, 2021.
- [82] E. Ryu, J. Liu, S. Wang, X. Chen, Z. Wang, and W. Yin, “Plug-and-play methods provably converge with properly trained denoisers,” in *International Conference on Machine Learning (ICML)*, 2019.
- [83] A. M. Teodoro, J. M. Bioucas-Dias, and M. A. T. Figueiredo, “Scene-adapted plug-and-play algorithm with convergence guarantees,” in *International Workshop on Machine Learning for Signal Processing (MLSP)*, 2017.
- [84] S. H. Chan, X. Wang, and O. A. Elgandy, “Plug-and-play admm for image restoration: Fixed-point convergence and applications,” *IEEE Transactions on Computational Imaging*, vol. 3, no. 1, pp. 84–98, 2016.
- [85] K. Gregor and Y. LeCun, “Learning fast approximations of sparse coding,” in *International Conference on Machine Learning (ICML)*, 2010.
- [86] B. Xin, Y. Wang, W. Gao, D. Wipf, and B. Wang, “Maximal sparsity with deep networks?” *Advances in Neural Information Processing Systems*, vol. 29, 2016.
- [87] J. Liu and X. Chen, “Alista: Analytic weights are as good as learned weights in lista,” in *International Conference on Learning Representations (ICLR)*, 2019.
- [88] X. Chen, J. Liu, Z. Wang, and W. Yin, “Theoretical linear convergence of unfolded ista and its practical weights and thresholds,” 2018.
- [89] J. R. Hershey, J. L. Roux, and F. Weninger, “Deep unfolding: Model-based inspiration of novel deep architectures,” *arXiv preprint arXiv:1409.2574*, 2014.
- [90] Z.-Q. Wang, J. L. Roux, D. Wang, and J. R. Hershey, “End-to-end speech separation with unfolded iterative phase reconstruction,” in *Conference of the International Speech Communication Association (INTERSPEECH)*, 2018.

- [91] K. Zhang, W. Zuo, S. Gu, and L. Zhang, “Learning deep cnn denoiser prior for image restoration,” in *Conference on Computer Vision and Pattern Recognition (CVPR)*, 2017.
- [92] T. Meinhardt, M. Moller, C. Hazirbas, and D. Cremers, “Learning proximal operators: Using denoising networks for regularizing inverse imaging problems,” in *International Conference on Computer Vision (ICCV)*, 2017.
- [93] J. H. R. Chang, C.-L. Li, B. Poczos, B. V. Kumar, and A. C. Sankaranarayanan, “One network to solve them all—solving linear inverse problems using deep projection models,” in *International Conference on Computer Vision (ICCV)*, 2017.
- [94] Y. Chen and T. Pock, “Trainable nonlinear reaction diffusion: A flexible framework for fast and effective image restoration,” *IEEE transactions on pattern analysis and machine intelligence*, vol. 39, no. 6, pp. 1256–1272, 2016.
- [95] S. Zheng, S. Jayasumana, B. Romera-Paredes, V. Vineet, Z. Su, D. Du, C. Huang, and P. H. Torr, “Conditional random fields as recurrent neural networks,” in *International Conference on Computer Vision (ICCV)*, 2015.
- [96] Z. Liu, X. Li, P. Luo, C. C. Loy, and X. Tang, “Deep learning markov random field for semantic segmentation,” *IEEE transactions on pattern analysis and machine intelligence*, vol. 40, no. 8, pp. 1814–1828, 2017.
- [97] C. J. Schuler, M. Hirsch, S. Harmeling, and B. Schölkopf, “Learning to deblur,” *IEEE transactions on pattern analysis and machine intelligence*, vol. 38, no. 7, pp. 1439–1451, 2015.
- [98] Y. Li, M. Tofghi, J. Geng, V. Monga, and Y. C. Eldar, “Efficient and interpretable deep blind image deblurring via algorithm unrolling,” *IEEE Transactions on Computational Imaging*, vol. 6, pp. 666–681, 2020.
- [99] Y. Yang, T. Liu, Y. Wang, J. Zhou, Q. Gan, Z. Wei, Z. Zhang, Z. Huang, and D. Wipf, “Graph neural networks inspired by classical iterative algorithms,” in *International Conference on Machine Learning (ICML)*, 2021.
- [100] X. Liu, W. Jin, Y. Ma, Y. Li, H. Liu, Y. Wang, M. Yan, and J. Tang, “Elastic graph neural networks,” in *International Conference on Machine Learning (ICML)*, 2021.
- [101] S. Chen, Y. C. Eldar, and L. Zhao, “Graph unrolling networks: Interpretable neural networks for graph signal denoising,” *IEEE Transactions on Signal Processing*, vol. 69, pp. 3699–3713, 2021.
- [102] J. Klicpera, A. Bojchevski, and S. Günnemann, “Predict then propagate: Graph neural networks meet personalized pagerank,” in *International Conference on Learning Representations*, 2019.
- [103] B. Chamberlain, J. Rowbottom, M. I. Gorinova, M. Bronstein, S. Webb, and E. Rossi, “Grand: Graph neural diffusion,” in *International Conference on Machine Learning*. PMLR, 2021, pp. 1407–1418.
- [104] M. Thorpe, T. M. Nguyen, H. Xia, T. Strohmer, A. Bertozzi, S. Osher, and B. Wang, “Grand++: Graph neural diffusion with a source term,” in *International Conference on Learning Representations*, 2022.
- [105] S. Bai, J. Z. Kolter, and V. Koltun, “Deep equilibrium models,” *Advances in Neural Information Processing Systems (NeurIPS)*, 2019.
- [106] L. El Ghaoui, F. Gu, B. Travacca, A. Askari, and A. Tsai, “Implicit deep learning,” *SIAM Journal on Mathematics of Data Science*, vol. 3, no. 3, pp. 930–958, 2021.
- [107] H. Dai, Z. Kozareva, B. Dai, A. Smola, and L. Song, “Learning steady-states of iterative algorithms over graphs,” in *International Conference on Machine Learning (ICML)*, 2018.
- [108] J. Liu, K. Kawaguchi, B. Hooi, Y. Wang, and X. Xiao, “Eignn: Efficient infinite-depth graph neural networks,” *Advances in Neural Information Processing Systems (NeurIPS)*, 2021.
- [109] F. Gu, H. Chang, W. Zhu, S. Sojoudi, and L. El Ghaoui, “Implicit graph neural networks,” *Advances in Neural Information Processing Systems (NeurIPS)*, 2020.
- [110] Y. Yang, Y. Wang, Z. Huang, and D. Wipf, “Implicit vs unfolded graph neural networks,” *arXiv preprint arXiv:2111.06592*, 2021.
- [111] I. Amburg, N. Veldt, and A. R. Benson, “Clustering in graphs and hypergraphs with categorical edge labels,” in *Proceedings of The Web Conference*, 2020.

- [112] P. S. Chodrow, N. Veldt, and A. R. Benson, “Hypergraph clustering: from blockmodels to modularity,” *Science Advances*, 2021.
- [113] J. H. Fowler, “Legislative cosponsorship networks in the us house and senate,” *Social networks*, vol. 28, no. 4, pp. 454–465, 2006.
- [114] —, “Connecting the congress: A study of cosponsorship networks,” *Political Analysis*, vol. 14, no. 4, pp. 456–487, 2006.
- [115] Y. Deshpande, S. Sen, A. Montanari, and E. Mossel, “Contextual stochastic block models,” in *Advances in Neural Information Processing Systems (NeurIPS)*, 2018.
- [116] D. Ghoshdastidar and A. Dukkipati, “Consistency of spectral partitioning of uniform hypergraphs under planted partition model,” *Advances in Neural Information Processing Systems (NeurIPS)*, 2014.
- [117] I. C. C.-Y. Lin and I.-H. Wang, “Community detection in hypergraphs: Optimal statistical limit and efficient algorithms,” in *International Conference on Artificial Intelligence and Statistics (AISTATS)*, 2018.
- [118] T. Chen, S. Kornblith, M. Norouzi, and G. Hinton, “A simple framework for contrastive learning of visual representations,” in *International Conference on Machine Learning (ICML)*, 2020.
- [119] R. L. Murphy, B. Srinivasan, V. Rao, and B. Ribeiro, “Janossy pooling: Learning deep permutation-invariant functions for variable-size inputs,” in *International Conference on Learning Representations (ICLR)*, 2018.

A Derivation of Eq. 3 and 4

We derive iterative update Eq. 3 and 4 as follows. Recall that our problem is defined as:

$$\min_{\mathbf{H}} \sum_{v \in \mathcal{V}} f(\mathbf{h}_v; \mathbf{x}_v) + \sum_{e \in \mathcal{E}} g_e(\mathbf{H}_e)$$

where $\mathbf{H} \in \mathbb{R}^N$ is the node feature matrix. $\mathbf{H}_e = [\mathbf{h}_{e,1} \ \cdots \ \mathbf{h}_{e,|e|}]^\top \in \mathbb{R}^{|e|}$ collects the associated node features inside edge e , where $\mathbf{h}_{e,i}$ corresponds to the node features of the i -th node in edge e . We use \mathbf{x}_v to denote the (initial) attribute of node v . Here, neither $f(\cdot; \mathbf{x}_v)$ nor $g_e(\cdot)$ is necessarily continuous. To solve such problem, we borrow the idea from ADMM [63]. We introduce an auxiliary variable $\mathbf{R}_e = \mathbf{H}_e$ for every $e \in \mathcal{E}$ and reformulate the problem as a constrained optimization problem:

$$\begin{aligned} \min_{\mathbf{H}} \sum_{v \in \mathcal{V}} f(\mathbf{h}_v; \mathbf{x}_v) + \sum_{e \in \mathcal{E}} g_e(\mathbf{R}_e) \\ \text{subject to } \mathbf{R}_e - \mathbf{H}_e = \mathbf{0}, \forall e \in \mathcal{E} \end{aligned}$$

By the Augmented Lagrangian Method (ALM), we assign a Lagrangian multiplier \mathbf{S}_e (scaled by $1/\lambda$) for each edge, then the objective function becomes:

$$\max_{\{\mathbf{S}_e\}_{e \in \mathcal{E}}} \min_{\mathbf{H}, \{\mathbf{R}_e\}_{e \in \mathcal{E}}} \sum_{v \in \mathcal{V}} f(\mathbf{h}_v; \mathbf{x}_v) + \sum_{e \in \mathcal{E}} g(\mathbf{R}_e) + \frac{\lambda}{2} \sum_{e \in \mathcal{E}} \|\mathbf{R}_e - \mathbf{H}_e + \mathbf{S}_e\|_F^2 - \frac{\lambda}{2} \sum_{e \in \mathcal{E}} \|\mathbf{S}_e\|_F^2. \quad (6)$$

We can iterate the following primal-dual steps to optimize Eq. 6. The primal step can be computed in a block-wise sense:

$$\begin{aligned} \mathbf{R}_e^{(t+1)} &\leftarrow \arg \min_{\mathbf{R}_e} \left\{ \frac{\lambda}{2} \|\mathbf{R}_e - \mathbf{H}_e^{(t)} + \mathbf{S}_e^{(t)}\|_F^2 + g(\mathbf{R}_e) \right\} \\ &= \mathbf{prox}_{g/\lambda} \left(\mathbf{H}_e^{(t)} - \mathbf{S}_e^{(t)} \right), \forall e \in \mathcal{E}, \end{aligned} \quad (7)$$

$$\begin{aligned} \mathbf{h}_v^{(t+1)} &\leftarrow \arg \min_{\mathbf{h}_v} \left\{ \frac{\lambda}{2} \sum_{e: v \in e} \|\mathbf{h}_v - \mathbf{S}_{e,v}^{(t)} - \mathbf{R}_{e,v}^{(t+1)}\|_F^2 + f(\mathbf{h}_v; \mathbf{x}_v) \right\} \\ &= \mathbf{prox}_{f(\cdot; \mathbf{x}_v)/\lambda d_v} \left(\frac{\sum_{e: v \in e} (\mathbf{S}_{e,v}^{(t)} + \mathbf{R}_{e,v}^{(t+1)})}{d_v} \right), \forall v \in \mathcal{V}. \end{aligned} \quad (8)$$

The dual step can be computed as:

$$\mathbf{S}_e^{(t+1)} \leftarrow \mathbf{S}_e^{(t)} + \mathbf{R}_e^{(t+1)} - \mathbf{H}_e^{(t+1)}, \forall e \in \mathcal{E}. \quad (9)$$

Denote $\mathbf{Q}_e^{(t+1)} := \mathbf{S}_e^{(t)} + \mathbf{R}_e^{(t+1)}$ and $\eta := 1/\lambda$, then the iterative updates become:

$$\mathbf{Q}_e^{(t+1)} = \mathbf{prox}_{\eta g} (2\mathbf{H}_e^{(t)} - \mathbf{Q}_e^{(t)}) + \mathbf{Q}_e^{(t)} - \mathbf{H}_e^{(t)}, \text{ for } e \in \mathcal{E}, \quad (10)$$

$$\mathbf{h}_v^{(t+1)} = \mathbf{prox}_{\eta f(\cdot; \mathbf{x}_v)/d_v} \left(\frac{\sum_{e: v \in e} \mathbf{Q}_{e,v}^{(t+1)}}{d_v} \right), \text{ for } v \in \mathcal{V}. \quad (11)$$

B Deferred Proofs

B.1 Proof of Proposition 2

Proof. Define $\pi : [K] \rightarrow [K]$ be an index mapping associated with the permutation matrix $\mathbf{P} \in \Pi(K)$ such that $\mathbf{PZ} = [\mathbf{z}_{\pi(1)}, \dots, \mathbf{z}_{\pi(K)}]^\top$. To prove that $\nabla g(\cdot)$ is permutation equivariant, we show by using the definition of partial derivatives. For any $\mathbf{Z} = [\mathbf{z}_1 \ \cdots \ \mathbf{z}_K]^\top$, and permutation π , we have:

$$\begin{aligned} [\nabla g(\mathbf{PZ})]_i &= \lim_{\delta \rightarrow 0} \frac{g(\mathbf{z}_{\pi(1)}, \dots, \mathbf{z}_{\pi(i)} + \delta, \dots, \mathbf{z}_{\pi(K)}) - g(\mathbf{z}_{\pi(1)}, \dots, \mathbf{z}_{\pi(i)}, \dots, \mathbf{z}_{\pi(K)})}{\delta} \\ &= \lim_{\delta \rightarrow 0} \frac{g(\mathbf{z}_1, \dots, \mathbf{z}_{\pi(i)} + \delta, \dots, \mathbf{z}_K) - g(\mathbf{z}_1, \dots, \mathbf{z}_{\pi(i)}, \dots, \mathbf{z}_K)}{\delta} \\ &= [\nabla g(\mathbf{Z})]_{\pi(i)}, \end{aligned} \quad (12)$$

where the second equality Eq. 12 is due to the permutation invariance of $g(\cdot)$. To prove Proposition 2 for the proximal gradient, we first define: $\mathbf{H}^* = \mathbf{prox}_g(\mathbf{Z}) = \arg \min_{\mathbf{H}} g(\mathbf{H}) + \frac{1}{2} \|\mathbf{H} - \mathbf{Z}\|_F^2$ for some \mathbf{Z} . For arbitrary permutation matrix $\mathbf{P} \in \Pi(K)$, we have

$$\begin{aligned} \mathbf{prox}_g(\mathbf{PZ}) &= \arg \min_{\mathbf{H}} g(\mathbf{H}) + \frac{1}{2} \|\mathbf{H} - \mathbf{PZ}\|_F^2 = \arg \min_{\mathbf{H}} g(\mathbf{H}) + \frac{1}{2} \|\mathbf{P}(\mathbf{P}^\top \mathbf{H} - \mathbf{Z})\|_F^2 \\ &= \arg \min_{\mathbf{H}} g(\mathbf{H}) + \frac{1}{2} \|\mathbf{P}^\top \mathbf{H} - \mathbf{Z}\|_F^2 = \arg \min_{\mathbf{H}} g(\mathbf{P}^\top \mathbf{H}) + \frac{1}{2} \|\mathbf{P}^\top \mathbf{H} - \mathbf{Z}\|_F^2 \\ &= \mathbf{PH}^*, \end{aligned} \tag{13}$$

where Eq. 13 is due to the permutation invariance of $g(\cdot)$. \square

B.2 Proof of Theorem 1

Proof. To prove Theorem 1, we first summarize one of our key results in the following Lemma 2.

Lemma 2. $\psi(\cdot) : [0, 1]^K \rightarrow \mathbb{R}^K$ is a permutation-equivariant function if and only if there is a function $\rho(\cdot) : [0, 1]^K \rightarrow \mathbb{R}$ that is permutation invariant to the last $K - 1$ entries, such that $[\psi(\mathbf{Z})]_i = \rho(\mathbf{z}_i, \underbrace{\mathbf{z}_{i+1}, \dots, \mathbf{z}_K}_{K-1}, \dots, \mathbf{z}_{i-1})$ for any i .

Proof. (Sufficiency) Define $\pi : [K] \rightarrow [K]$ be an index mapping associated with the permutation matrix $\mathbf{P} \in \Pi(K)$ such that $\mathbf{PZ} = [\mathbf{z}_{\pi(1)}, \dots, \mathbf{z}_{\pi(K)}]^\top$. Then $[\psi(\mathbf{z}_{\pi(1)}, \dots, \mathbf{z}_{\pi(K)})]_i = \rho(\mathbf{z}_{\pi(i)}, \mathbf{z}_{\pi(i+1)}, \dots, \mathbf{z}_{\pi(K)}, \dots, \mathbf{z}_{\pi(i-1)})$. Since $\rho(\cdot)$ is invariant to the last $K - 1$ entries, $[\psi(\mathbf{PZ})]_i = \rho(\mathbf{z}_{\pi(i)}, \mathbf{z}_{\pi(i+1)}, \dots, \mathbf{z}_K, \dots, \mathbf{z}_{\pi(i-1)}) = [\psi(\mathbf{Z})]_{\pi(i)}$.

(Necessity) Given a permutation-equivariant function $\psi : [0, 1]^K \rightarrow \mathbb{R}^K$, we first expand it to the following form: $[\psi(\mathbf{Z})]_i = \rho_i(\mathbf{z}_1, \dots, \mathbf{z}_K)$. Permutation-equivariance means $\rho_{\pi(i)}(\mathbf{z}_1, \dots, \mathbf{z}_K) = \rho_i(\mathbf{z}_{\pi(1)}, \dots, \mathbf{z}_{\pi(K)})$. Suppose given an index i , consider any permutation $\pi : [K] \rightarrow [K]$, where $\pi(i) = i$. Then, we have $\rho_i(\mathbf{z}_1, \dots, \mathbf{z}_i, \dots, \mathbf{z}_K) = \rho_{\pi(i)}(\mathbf{z}_1, \dots, \mathbf{z}_i, \dots, \mathbf{z}_K) = \rho_i(\mathbf{z}_{\pi(1)}, \dots, \mathbf{z}_i, \dots, \mathbf{z}_{\pi(K)})$, which implies $\rho_i : \mathbb{R}^K \rightarrow \mathbb{R}$ must be invariant to the $K - 1$ elements other than the i -th element. Now, consider a permutation π where $\pi(1) = i$. Then $\rho_i(\mathbf{z}_1, \mathbf{z}_2, \dots, \mathbf{z}_K) = \rho_{\pi(1)}(\mathbf{z}_1, \mathbf{z}_2, \dots, \mathbf{z}_K) = \rho_1(\mathbf{z}_{\pi(1)}, \mathbf{z}_{\pi(2)}, \dots, \mathbf{z}_{\pi(K)}) = \rho_1(\mathbf{z}_i, \mathbf{z}_{i+1}, \dots, \mathbf{z}_K, \dots, \mathbf{z}_{i-1})$, where the last equality is due to our previous argument. This implies two results. First, for all i , $\rho_i(\mathbf{z}_1, \mathbf{z}_2, \dots, \mathbf{z}_i, \dots, \mathbf{z}_K), \forall i \in [K]$ should be written in terms of $\rho_1(\mathbf{z}_i, \mathbf{z}_{i+1}, \dots, \mathbf{z}_K, \dots, \mathbf{z}_{i-1})$. Moreover, ρ_1 is permutation invariant to its last $K - 1$ entries. Therefore, we just need to set $\rho = \rho_1$ and broadcast it accordingly to all entries. We conclude the proof. \square

To proceed the proof, we bring in the following mathematical tools [50]:

Definition 5. Given a vector $\mathbf{z} = [\mathbf{z}_1, \dots, \mathbf{z}_K]^\top \in \mathbb{R}^K$, we define power mapping $\phi_M : \mathbb{R} \rightarrow \mathbb{R}^M$ as $\phi_M(z) = [z \ z^2 \ \dots \ z^M]^\top$, and sum-of-power mapping $\Phi_M : \mathbb{R}^K \rightarrow \mathbb{R}^M$ as $\Phi_M(\mathbf{z}) = \sum_{i=1}^K \phi_M(\mathbf{z}_i)$, where M is the largest degree.

Lemma 3. Let $\mathcal{X} = \{[\mathbf{z}_1, \dots, \mathbf{z}_K]^\top \in [0, 1]^K \text{ such that } \mathbf{z}_1 < \mathbf{z}_2 < \dots < \mathbf{z}_K\}$. We define mapping $\tilde{\phi} : \mathbb{R} \rightarrow \mathbb{R}^{K+1}$ as $\tilde{\phi}(z) = [z^0 \ z^1 \ z^2 \ \dots \ z^K]^\top$, and mapping $\tilde{\Phi} : \mathbb{R}^K \rightarrow \mathbb{R}^{K+1}$ as $\tilde{\Phi}(\mathbf{z}) = \sum_{i=1}^K \tilde{\phi}(\mathbf{z}_i)$, where M is the largest degree. Then $\tilde{\Phi}$ restricted on \mathcal{X} , i.e., $\tilde{\Phi} : \mathcal{X} \rightarrow \mathbb{R}^{K+1}$, is a homeomorphism.

Proof. Proved in Lemma 6 in [50]. \square

We note that Definition 5 is slightly different from the mappings defined in Lemma 3 [50] as it removes the constant (zero-order) term. Combining with Lemma 3 [50] and results in [66], we have the following result:

Lemma 4. Let $\mathcal{X} = \{[z_1, \dots, z_K]^\top \in [0, 1]^K \text{ such that } z_1 < z_2 < \dots < z_K\}$, then there exists a homeomorphism $\Phi_M : \mathcal{X} \rightarrow \mathbb{R}^M$ such that $\Phi_M(\mathbf{z}) = \sum_{i=1}^K \phi_M(\mathbf{z}_i)$ where $\phi_M : \mathbb{R} \rightarrow \mathbb{R}^M$ if $M \geq K$.

Proof. For $M = K$, we choose ϕ_K and Φ_K to be the power mapping and power sum with largest degree K defined in Definition 5. We note that $\tilde{\Phi}(\mathbf{z}) = [K \ \Phi_K(\mathbf{z})^\top]^\top$. Since K is a constant, there exists a homeomorphism between the images of $\tilde{\Phi}(\mathbf{z})$ and $\Phi_K(\mathbf{z})$. By Lemma 3, $\tilde{\Phi} : \mathcal{X} \rightarrow \mathbb{R}^{K+1}$ is a homeomorphism, which implies $\Phi_K(\mathbf{z}) : \mathcal{X} \rightarrow \mathbb{R}^K$ is also a homeomorphism.

For $M > K$, we first pad every input $\mathbf{z} \in \mathcal{X}$ with a constant $k > 1$ to be an M -dimension $\hat{\mathbf{z}} \in \mathbb{R}^M$. Note that padding is homeomorphic since k is a constant. All such $\hat{\mathbf{z}}$ form a subset $\mathcal{X}' \subset \{[z_1, \dots, z_M]^\top \in [0, k]^M \text{ such that } z_1 < z_2 < \dots < z_M\}$. We choose $\hat{\phi} : \mathbb{R} \rightarrow \mathbb{R}^M$ to be power mapping and $\hat{\Phi} : \mathcal{X}' \rightarrow \mathbb{R}^M$ to be sum-of-power mapping restricted on \mathcal{X}' , respectively. Following [66], we construct $\Phi_M(\mathbf{z})$ as below:

$$\hat{\Phi}_M(\hat{\mathbf{z}}) = \sum_{i=1}^K \hat{\phi}_M(\mathbf{z}_i) + \sum_{i=K+1}^M \hat{\phi}_M(k) = \sum_{i=1}^K \hat{\phi}_M(\mathbf{z}_i) + \sum_{i=1}^M \hat{\phi}_M(k) - \sum_{i=1}^K \hat{\phi}_M(k) \quad (14)$$

$$= \sum_{i=1}^K (\hat{\phi}_M(\mathbf{z}_i) - \hat{\phi}_M(k)) + \sum_{i=1}^M \hat{\phi}_M(k) = \sum_{i=1}^K (\hat{\phi}_M(\mathbf{z}_i) - \hat{\phi}_M(k)) + M\hat{\phi}_M(k), \quad (15)$$

which induces $\sum_{i=1}^K (\hat{\phi}_M(\mathbf{z}_i) - \hat{\phi}_M(k)) = \hat{\Phi}_M(\hat{\mathbf{z}}) - M\hat{\phi}_M(k)$. Let $\phi_M(\mathbf{z}) = \hat{\phi}_M(\mathbf{z}_i) - \hat{\phi}_M(k)$, and $\Phi_M(\mathbf{z}) = \sum_{i=1}^K \phi_M(\mathbf{z}_i)$. Since $[0, k]$ is naturally homeomorphic to $[0, 1]$, by our argument for $M = K$, $\hat{\Phi}_M : \mathcal{X}' \rightarrow \mathbb{R}^M$ is a homeomorphism. This implies $\Phi_M : \mathcal{X} \rightarrow \mathbb{R}^M$ is also a homeomorphism. \square

It is straightforward to show the sufficiency of Theorem 1 by verifying that for arbitrary permutation $\pi : [K] \rightarrow [K]$, $[\psi(\mathbf{z}_{\pi(1)}, \dots, \mathbf{z}_{\pi(K)})]_i = \rho(\mathbf{z}_{\pi(i)}, \sum_{j=1}^K \phi(\mathbf{z}_j)) = [\psi(\mathbf{z}_1, \dots, \mathbf{z}_K)]_{\pi(i)}$. With Lemma 2 and 4, we can conclude the necessity of Theorem 1 by the following construction:

1. By Lemma 2, any permutation equivariant function $\psi(\mathbf{z}_1, \dots, \mathbf{z}_K)$ can be written as $[\psi(\cdot)]_i = \tau(\mathbf{z}_i, \mathbf{z}_{i+1}, \dots, \mathbf{z}_K, \dots, \mathbf{z}_{i-1})$ such that $\tau(\cdot)$ is invariant to the last $K - 1$ elements.
2. By Lemma 4, we know that there exists a homeomorphism mapping Φ_K which is continuous, invertible, and invertibly continuous. For arbitrary $\mathbf{z} \in [0, 1]^K$, the difference between \mathbf{z} and $\Phi_K^{-1} \circ \Phi_K(\mathbf{z})$ is up to a permutation.
3. Since $\tau(\cdot)$ is permutation invariant to the last $K - 1$ elements, we can construct the function $\tau(\mathbf{z}_i, \mathbf{z}_{i+1}, \dots, \mathbf{z}_K, \dots, \mathbf{z}_{i-1}) = \tau(\mathbf{z}_i, \Phi_{K-1}^{-1} \circ \Phi_{K-1}(\mathbf{z}_{i+1}, \dots, \mathbf{z}_K, \dots, \mathbf{z}_{i-1})) = \tilde{\rho}(\mathbf{z}_i, \sum_{j \neq i} \phi_{K-1}(\mathbf{z}_j)) = \rho(\mathbf{z}_i, \sum_{j=1}^K \phi_{K-1}(\mathbf{z}_j))$, where $\tilde{\rho}(x, \mathbf{y}) = \tau(x, \Phi_{K-1}^{-1}(\mathbf{y}))$ and $\rho(x, \mathbf{y}) = \tilde{\rho}(x, \mathbf{y} - \phi_{K-1}(x))$.

Since τ , Φ_{K-1}^{-1} , and ϕ_{K-1} are all continuous functions, their composition ρ is also continuous. \square

C Additional Experiments and Details

C.1 Experiments on ED-HNNII

As we described in Sec. 3.2, an extension to our ED-HNN is to consider $\mathcal{V} \rightarrow \mathcal{E}$ message passing and $\mathcal{E} \rightarrow \mathcal{V}$ message passing as two equivariant set functions. The detailed algorithm is illustrated in **Algorithm 2**, where the red box highlights the major difference with ED-HNN.

In our tested datasets, hyperedges do not have initial attributes. In our implementation, we assign a common learnable vector for every hyperedge as their first-layer features $\mathbf{m}_{u \rightarrow e}^{(0)}$. The performance of ED-HNNII and the comparison with other baselines are presented in Table 4. Our finding is that

Algorithm 2: ED-HNNII**Initialization:** $H^{(0)} = X$ and three MLPs $\hat{\phi}, \hat{\rho}, \hat{\psi}$ (shared across L layers).**For** $t = 0, 1, 2, \dots, L - 1$, **do:**

1. Designing the messages from \mathcal{V} to \mathcal{E} : $\mathbf{m}_{u \rightarrow e}^{(t)} = \hat{\phi}(\mathbf{m}_{u \rightarrow e}^{(t-1)}, \mathbf{h}_u^{(t)})$, for all $u \in \mathcal{V}$.
2. Sum $\mathcal{V} \rightarrow \mathcal{E}$ messages over hyperedges $\mathbf{m}_e^{(t)} = \sum_{u \in e} \mathbf{m}_{u \rightarrow e}^{(t)}$, for all $e \in \mathcal{E}$.
3. Broadcast $\mathbf{m}_e^{(t)}$ and design the messages from \mathcal{E} to \mathcal{V} : $\mathbf{m}_{e \rightarrow v}^{(t)} = \hat{\rho}(\mathbf{h}_v^{(t)}, \mathbf{m}_e^{(t)})$, for all $v \in e$.
4. Update $\mathbf{h}_v^{(t+1)} = \hat{\psi}(\mathbf{h}_v^{(t)}, \sum_{e: u \in e} \mathbf{m}_{e \rightarrow u}^{(t)}, \mathbf{x}_v, d_v)$, for all $v \in \mathcal{V}$.

Table 4: Additional experiments and updated leaderboard with ED-HNNII. Prediction accuracy (%). **Bold font** highlights when ED-HNNII outperforms the original ED-HNN. Other details are kept consistent with Table 2.

	Cora	Citeseer	Pubmed	Cora-CA	DBLP-CA	Training Time (10^{-1} s)
HGNN [25]	79.39 \pm 1.36	72.45 \pm 1.16	86.44 \pm 0.44	82.64 \pm 1.65	91.03 \pm 0.20	0.24 \pm 0.51
HCHA [27]	79.14 \pm 1.02	72.42 \pm 1.42	86.41 \pm 0.36	82.55 \pm 0.97	90.92 \pm 0.22	0.24 \pm 0.01
HNHN [24]	76.36 \pm 1.92	72.64 \pm 1.57	86.90 \pm 0.30	77.19 \pm 1.49	86.78 \pm 0.29	0.30 \pm 0.56
HyperGCN [23]	78.45 \pm 1.26	71.28 \pm 0.82	82.84 \pm 8.67	79.48 \pm 2.08	89.38 \pm 0.25	0.42 \pm 1.51
UniGCNII [25]	78.81 \pm 1.05	73.05 \pm 2.21	88.25 \pm 0.40	83.60 \pm 1.14	91.69 \pm 0.19	4.36 \pm 1.18
AllDeepSets [26]	76.88 \pm 1.80	70.83 \pm 1.63	88.75 \pm 0.33	81.97 \pm 1.50	91.27 \pm 0.27	1.23 \pm 1.09
AllSetTransformer [26]	78.58 \pm 1.47	73.08 \pm 1.20	88.72 \pm 0.37	83.63 \pm 1.47	91.53 \pm 0.23	1.64 \pm 1.63
ED-HNN	80.31 \pm 1.35	73.70 \pm 1.38	89.03 \pm 0.53	83.97 \pm 1.55	91.90 \pm 0.19	1.71 \pm 1.13
ED-HNNII	78.47 \pm 1.62	72.65 \pm 1.56	89.56 \pm 0.62	82.17 \pm 1.68	91.93 \pm 0.29	1.85 \pm 1.09
	Congress	Senate	Walmart	House	Avg. Rank	Inference Time (10^{-2} s)
HGNN [25]	91.26 \pm 1.15	48.59 \pm 4.52	62.00 \pm 0.24	61.39 \pm 2.96	5.67	1.01 \pm 0.04
HCHA [27]	90.43 \pm 1.20	48.62 \pm 4.41	62.35 \pm 0.26	61.36 \pm 2.53	6.22	1.54 \pm 0.18
HNHN [24]	53.35 \pm 1.45	50.93 \pm 6.33	47.18 \pm 0.35	67.80 \pm 2.59	7.11	8.11 \pm 0.05
HyperGCN [23]	55.12 \pm 1.96	42.45 \pm 3.67	44.74 \pm 2.81	48.32 \pm 2.93	8.33	0.87 \pm 0.06
UniGCNII [25]	94.81 \pm 0.81	49.30 \pm 4.25	54.45 \pm 0.37	67.25 \pm 2.57	4.33	21.22 \pm 0.13
AllDeepSets [26]	91.80 \pm 1.53	48.17 \pm 5.67	64.55 \pm 0.33	67.82 \pm 2.40	5.89	5.35 \pm 0.33
AllSetTransformer [26]	92.16 \pm 1.05	51.83 \pm 5.22	65.46 \pm 0.25	69.33 \pm 2.20	3.33	6.06 \pm 0.67
ED-HNN	95.00 \pm 0.99	64.79 \pm 5.14	66.91 \pm 0.41	72.45 \pm 2.28	1.56	5.87 \pm 0.36
ED-HNNII	95.19 \pm 1.34	63.81 \pm 6.17	67.24 \pm 0.45	73.95 \pm 1.97	2.56	6.07 \pm 0.40

ED-HNNII can outperform ED-HNN on datasets with relatively larger scale or more heterophily. And the average accuracy improvement by ED-HNNII is around 0.5%. We argue that ED-HNNII inherently has more complex computational mechanism, and thus tends to overfit on small datasets (e.g., Cora, Citeseer, etc.). Moreover, superior performance on heterophilic datasets also implies that injecting more equivariance benefits handling heterophilic data. From Table 4, the measured computational efficiency is also comparable to ED-HNN and other baselines.

C.2 Details of Benchmarking Datasets

Our benchmark datasets consist of existing seven datasets (Cora, Citeseer, Pubmed, Cora-CA, DBLP-CA, Walmart, and House) from [26], and two newly introduced datasets (Congress [114] and Senate [113]). For existing datasets, we downloaded the processed version by [26]. For Congress [114] and Senate [113], we used the same setting as [72]. In Congress dataset, nodes are US Congresspersons and hyperedges are comprised of the sponsor and co-sponsors of legislative bills put forth in both the House of Representatives and the Senate. In Senate dataset, nodes are US Congresspersons and hyperedges are comprised of the sponsor and co-sponsors of bills put forth in the Senate. Each node in both datasets is labeled with political party affiliation. Both datasets were from James Fowler’s data [113, 114]. We also list more detailed statistical information on the tested datasets in Table 5.

C.3 Hyperparameters for Benchmarking Datasets

For a fair comparison, we use the same training recipe for all the models. For baseline models, we precisely follow the hyperparameter settings from [26]. For ED-HNN, we adopt Adam optimizer with fixed learning rate=0.001 and weight decay=0.0, and train for 500 epochs for all datasets. The standard deviation is reported by repeating experiments on ten different data splits. We fix the input dropout rate to be 0.2, and dropout rate to be 0.3. For internal MLPs, we add a LayerNorm for each layer similar to [26]. Other parameters regarding model sizes are obtained by grid search, which are enumerated in Table 6. The search range of layer number is {1, 2, 4, 6, 8} and the hidden dimension is {96, 128, 256, 512}. We find the model size is proportional to the dataset scale, and in general

Table 5: More dataset statistics. CE homophily is the homophily score [68] based on CE of hypergraphs.

	Cora	Citeseer	Pubmed	Cora-CA	DBLP-CA	Congress	Senate	Walmart	House
# nodes	2708	3312	19717	2708	41302	1718	282	88860	1290
# hyperedges	1579	1079	7963	1072	22363	83105	315	69906	340
# features	1433	3703	500	1433	1425	100	100	100	100
# classes	7	6	3	7	6	2	2	11	2
avg. d_v	2.767	2.043	2.756	2.693	3.411	427.251	20.177	6.184	10.180
avg. $ e $	1.748	1.541	1.963	1.929	2.213	8.654	9.531	3.461	8.056
CE Homophily	0.897	0.893	0.952	0.803	0.869	0.555	0.498	0.530	0.509

heterophilic data need deeper architecture. For ED-HNNII, due to the inherent model complexity, we need to prune model depth and width to fit each dataset.

Algorithm 3: Contextual Hypergraph Stochastic Block Model

Initialization: Empty hyperedge set $\mathcal{E} = \emptyset$. Draw vertex set \mathcal{V}_1 of 2,500 nodes with class 1.

Draw vertex set \mathcal{V}_2 of 2,500 nodes with class 2.

For $i = 0, 1, 2, \dots, 1,000$, **do:**

1. Sample a subset e_1 with α_1 nodes from \mathcal{V}_1 .
 2. Sample a subset e_2 with α_2 nodes from \mathcal{V}_2 .
 3. Construct the hyperedge $\mathcal{E} \leftarrow \mathcal{E} \cup \{e_1 \cup e_2\}$.
-

Table 6: Choice of hyperparameters for ED-HNN. # is short for “number of”, hd. stands for hidden dimension, cls. means the classifier. When number of MLP layers equals to 0, the MLP boils down to be an identity mapping.

ED-HNN	Cora	Citeseer	Pubmed	Cora-CA	DBLP-CA	Congress	Senate	Walmart	House
# iterations	1	1	8	1	1	4	8	6	8
# layers of $\hat{\phi}$	0	0	2	1	1	2	2	2	2
# layers of $\hat{\rho}$	1	1	2	1	1	2	2	2	2
# layers of $\hat{\varphi}$	1	1	1	1	1	2	2	2	2
# layer cls.	1	1	2	2	2	2	2	2	2
MLP hd.	256	256	512	128	128	156	512	512	256
cls. hd.	256	256	256	96	96	128	256	256	128

ED-HNNII	Cora	Citeseer	Pubmed	Cora-CA	DBLP-CA	Congress	Senate	Walmart	House
# iterations	1	1	4	1	1	4	4	4	4
# layers of $\hat{\phi}$	1	1	2	1	1	2	2	2	2
# layers of $\hat{\rho}$	1	1	2	1	1	2	2	2	2
# layers of $\hat{\varphi}$	0	1	1	1	1	1	1	1	1
# layer cls.	1	1	2	2	2	2	2	2	2
MLP hd.	128	128	512	128	128	156	512	512	256
cls. hd.	96	96	256	96	96	128	256	256	128

C.4 Synthetic Heterophilic Datasets

We use the contextual hypergraph stochastic block model [115–117] to synthesize data with controlled heterophily. The generated graph contains 5,000 nodes and two classes in total, and 2,500 nodes for each class. We construct hyperedges by randomly sampling α_1 nodes from class 1, and α_2 nodes from class 2 without replacement. Each hyperedge has a fixed cardinality $|e| = \alpha_1 + \alpha_2 = 15$. We draw 1,000 hyperedges in total. The detailed data synthesis pipeline is summarized in **Algorithm 3**. We use $\alpha = \min\{\alpha_1, \alpha_2\}$ to characterize the heterophily level of the hypergraph. For a more intuitive illustration, we list the CE homophily corresponding to different α in Table 7. Experiments on synthetic heterophilic datasets fix the training hyperparameters and hidden dimension=256 to guarantee a fair parameter budget ($\sim 1M$). Baseline HNNs are all of one-layer architecture as they are not scalable with the depth shown in Sec. 5.3. Since our ED-HNN adopts parameter sharing scheme, we can easily repeat the diffusion layer twice to achieve better results without parameter overheads.

C.5 Synthetic Diffusion Datasets and Additional Experiments

In order to evaluate the ability of ED-HNN to express given hypergraph diffusion, we generate semi-synthetic diffusion data using the Senate hypergraph [112] and synthetic node features. The data consists of 1,000 pairs $(H^{(0)}, H^{(1)})$. The initial node features $H^{(0)}$ are sampled from 1-dim

Table 7: Correspondence between Heterophily α and CE Homophily.

α	1	2	3	4	6	7
CE Homophily	0.875	0.765	0.672	0.596	0.495	0.474

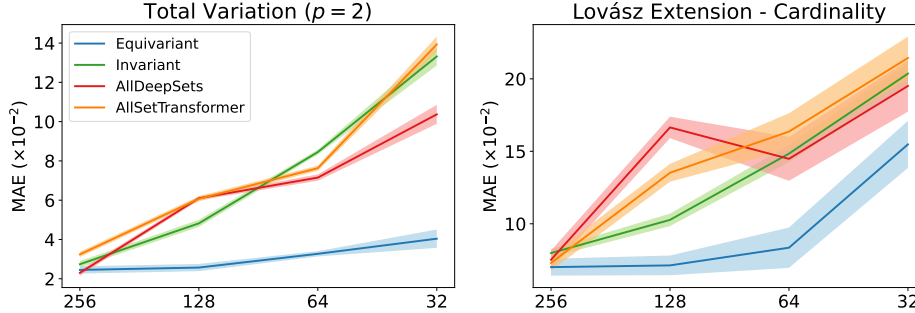


Figure 4: Comparing the Powers to Represent known Diffusion (using ADMM with the proximal operators in Eq. 3 and 4): MAE v.s. Latent Dimensions

Gaussian distributions with mean 0 and variance randomly drawn between 1 and 100. That is, to generate a single instance of $\mathbf{H}^{(0)}$, we first pick σ uniformly from $[1,10]$, and then sample the coordinate entries as $\mathbf{h}_v^{(0)} \sim N(0, \sigma^2)$. Then we apply the gradient step in Eq. 2 to obtain the corresponding $\mathbf{H}^{(1)}$. For non-differentiable node or edge potentials, we adopt subgradients for convenient computation. We fix the node potential as $f(\mathbf{h}_v; \mathbf{x}_v) = (\mathbf{h}_v - \mathbf{x}_v)^2$ where $\mathbf{x}_v \equiv \mathbf{h}_v^{(0)}$. We consider 3 different edge potentials from Example 1 with varying complexities: a) CE, b) TV ($p = 2$) and c) LEC ($p = 2$). For LEC, we set \mathbf{y} as follows: if $|e|$ is even, then $y_i = 2/|e|$ if $i \leq |e|/2$ and $-2/|e|$ otherwise; if $|e|$ is odd, then $y_i = 2/(|e| - 1)$ if $i \leq (|e| - 1)/2$, $y_i = 0$ if $i = (|e| + 1)/2$, and $y_0 = -2/(|e| - 1)$ otherwise. In order to apply the gradient step in Eq. 2 we need to specify the learning rate η . We choose η in a way such that $\text{Var}(\mathbf{H}^{(1)})/\text{Var}(\mathbf{H}^{(0)})$ does not vary too much among the three different edge potentials. Specifically, we set $\eta = 0.5$ for CE, $\eta = 0.02$ for TV and $\eta = 0.1$ for LEC.

Beyond semi-synthetic diffusion data generated from the gradient step Eq. 2, we also considered synthetic diffusion data obtained from the proximal operators Eq. 3 and 4. We generated a random uniform hypergraph with 1,000 nodes and 1,000 hyperedges of constant hyperedge size 20. The diffusion data on this hypergraph consists of 1,000 pairs $(\mathbf{H}^{(0)}, \mathbf{H}^{(1)})$. The initial node features $\mathbf{H}^{(0)}$ are sampled in the same way as before. We apply the updates given by Eq. 3 and 4 to obtain $\mathbf{H}^{(1)}$. We consider the same node potential and 2 edge potentials TV ($p = 2$) and LEC ($p = 2$). We set $\eta = 1/2$ for both cases. We show the results in Figure 4. The additional results resonate with our previous results in Figure 3. Again, our ED-HNN outperforms other baseline HNNs by a significant margin when hidden dimension is limited.

C.6 More Complexity Analysis

In this section, we provide more efficiency comparison with HyperSAGE [28] and LEGCN [30]. As we discussed in 3.4, HyperSAGE and LEGCN may be able to learn hyperedge equivariant operator. However, both HyperSAGE and LEGCN need to build node-hyperedge pair, which is memory consuming and unfriendly to efficient message passing implementation. To demonstrate this we compare the model our model with HyperSAGE and LEGCN in terms of training and inference efficiency. We reuse the official code provided in OpenReview to benchmark HyperSAGE. Since LEGCN has not released code, we reimplement it using Pytorch Geometric Library. We can only test the speed of these models on Cora dataset, because HyperSAGE and LEGCN cannot scale up as there is no efficient implementation yet for their computational prohibitive preprocessing procedures. The results are presented in Table 8. We note that HyperSAGE cannot easily employ message passing between \mathcal{V} and \mathcal{E} , since neighbor aggregation step in HyperSAGE needs to rule out the central node. Its official implementation adopts a naive “for”-loop for each forward pass which is unable to fully utilize the GPU parallelism and significant deteriorates the speed. LEGCN can be implemented via

message passing, however, the graphs expanded over node-edge pairs are much denser thus cannot scale up to larger dataset.

Table 8: Performance and Efficiency Comparison with HyperSAGE and LEGCN. The prediction accuracy of HyperSAGE is copied from the original manuscript [28].

	HyperSAGE [28]	LEGCN [30]	ED-HNN	ED-HNNII
Training Time (10^{-1} s)	43.93 ± 2.15	0.56 ± 0.71	0.15 ± 0.68	0.25 ± 0.48
Inference Time (10^{-2} s)	297.57 ± 30.57	0.42 ± 0.06	0.15 ± 0.03	0.20 ± 0.08
Prediction Accuracy (%)	69.30 ± 2.70	73.34 ± 1.06	80.31 ± 1.35	78.47 ± 1.62